Mathematical Modelling and Numerical Simulation with Applications, 2023, 3(1), 74–100

https://dergipark.org.tr/en/pub/mmnsa

ISSN Online: 2791-8564 / Open Access

https://doi.org/10.53391/mmnsa.1280184

RESEARCH PAPER

A modelling of bioconvective flow existing with tiny particles and quartic autocatalysis reaction across stratified upper horizontal surface of a paraboloid of revolution

Nehad Ali Shah [1,‡], **Amos Oladele Popoola** [2,‡], **Tosin Oreyeni** [3,*,‡], **Emmanuel Omokhuale** [4,‡] **and Muhammad Muhammad Altine** [5,‡]

[1]Department of Mechanical Engineering, Sejong University, Seoul 05006, South Korea, [2]Department of Mathematical Sciences, Osun State University, Osogbo, Nigeria, [3]Department of Physical Sciences, Mathematics Programme Unit, Precious Cornerstone University, Ibadan, Nigeria, [4]Department of Mathematical Sciences, Federal University Gusau, Nigeria, [5]Department of Mathematics, Federal University Birnin Kebbi, Kalgo, Nigeria

*Corresponding Author

‡nehadali199@sejong.ac.kr (Nehad Ali Shah); amos.popoola@uniosun.edu.ng (Amos Oladele Popoola); oreyenitos@gmail.com (Tosin Oreyeni); emmanuelomokhuale@yahoo.com (Emmanuel Omokhuale); altine@fubk.edu.ng (Muhammad Muhammad Altine)

Abstract

The study considers the case of the unequal diffusion coefficients of reactant A (bulk fluid) and reactant B (catalyst at the wall) with the dispersion of both nanoparticles and gyrotactic microorganisms of Erying-Powell fluid flow over a surface with non-uniform thickness in the presence of variable fluid properties and stratification. The numerical solution of the transformed governing equations is obtained by using the Runge-Kutta method and shooting techniques. The outcome of this study is that the increasing values of temperature-dependent thermal conductivity parameter lead to the augmentation of the kinetic energy which thereafter causes a significant enhancement of the fluid temperature.

Keywords: Darcy-Forchheimer; bioconvection; Erying-Powell fluid; stratification; nanofluids; autocatalysis; paraboloid of revolution

AMS 2020 Classification: 76D50; 35Q35; 76A05

1 Introduction

Stratification is an important component of heat and mass transfer which is referred to as the scientific or natural process that describes the production of layers of fluids as a result of the

➤ **Received:** 18.02.2023 ➤ **Revised:** 25.03.2023 ➤ **Accepted:** 27.03.2023 ➤ **Published:** 31.03.2023

mixing of various fluids with varied densities, temperature variances, and concentration differences. The idea behind this stratification phenomenon is useful in both natural and industrial processes such as the occurrence of flows in lakes, oceans, rivers, groundwater reservoirs, thermal energy storage systems, and heat release into the atmosphere. Recently, the effect of stratification on the hydromagnetic nanofluid flow along an exponentially stretching sensor plate was presented by Shamshuddin et al. [1]. Tamilzharasan et al. [2] discussed the mixed convention flow of Williamson fluid in a stratified porous medium. The impact of triple stratification on hydromagnetic flow with Soret and Dufour over a stretching cylinder was analyzed by Jagan et al. [3] Rehman et al. [4] studied thermally stratified Eyring-Powel fluid with melting heat phenomenon.

Oreyeni et al. [5] demonstrated the importance of triple stratifications in the dynamics of a micropolar fluid with nanoparticles and exponential heat production. They observed that increased stratification minimizes the temperature difference between the surface and the free stream, resulting in declination of fluid velocity and temperature. Olanrewaju et al. [6] analyzed the impact of double stratification and variable fluid properties on a chemically reacting upper-convected Maxwell fluid utilizing an analytic approach. The effect of stratification phenomena on a Sutterby nanofluid was discussed by Khan et al. [7]. Chen et al. [8] investigated thermophoretic Casson fluid flow with a magnetic dipole in a stratified environment. The bioconvective flow of Casson over a stratified cylinder was addressed by Dawar et al. [9]. Verma et al. [10] presented the existence of mixed convection and double stratification in Darcy-Forchheimer porous medium. The magnetohydrodynamic mixed convective flow of nanofluid with thermal stratification was considered by Mahmood et al. [11].

Nanofluid is defined as fluid with nanometer-sized particles suspended in conventional heat transfer fluids characterized by low thermal conductivity in order to improve the fluid's heat transfer efficiency. Researchers are interested in the flow of fluid when nanometer-sized particles are annotated in the flow field because of its vast variety of applications in biomedical and technical disciplines such as microelectronics, polymer extrusion, cancer treatment, safer surgery procedures, and microfluidics. Owing to a wide range of applications, nanofluid flow over various geometries has emerged as a fascinating and significant research area among academics. Koriko et al. [12] investigated the bioconvection flow of shear-thinning fluid employing active and passive controls of nanoparticles. It was observed that the presence of Brownian motion encourages the warming of particle molecules and increases thermal conductivity, resulting in an increase in fluid temperature. Shah et al. [13] analyzed the significance of Brownian motion and thermophoretic diffusion effects as major mechanisms for heat transfer in their study. Nadeem et al. [14] considered the numerical analysis for elastico-viscous fluid with the suspension of nanoparticles. Boundary layer flow of a nanofluid in the presence of variable suction and viscous dissipation over an exponentially stretched wall was discussed by Rao et al. [15]. Rasheed et al. [16] presented the significance of Joule heating on the hydromagnetic flow of Jeffery nanofluid flow over a stretching cylinder. Abbas et al. [17] studied the heat transfer of nanofluid along a vertical sheet with a magnetic effect. Other studies relating to the dynamics of nanofluid can be seen in [18–21].

The process by which one or more substances are changed into one or more new substances is known as a chemical reaction. During the course of a chemical reaction catalysis is known to be the process of accelerating the rate of the reaction by introducing a chemical component known as a catalyst which is frequently used to accelerate a chemical reaction. It is therefore believed that catalyzed reactions are classified into two types: homogeneously catalyzed reactions and heterogeneously catalyzed reactions. Both the reactant and the catalyst are present in the same phase in a homogeneously catalyzed reaction. This has a wide range of applications in

industry as it allows an increase in reaction rate without an increase in temperature. An example of homogeneous catalysis is the decomposition of ozone when Nitric oxide (NO) acts as a catalyst that affects the rate of the decomposition reaction. That is, $NO+O_3 \rightarrow NO_2+O_2$. When the reactant and catalyst are in separate stages the reaction is called heterogeneous catalyzed. The catalyst stays solid in this type of reaction whereas the reactants are gaseous or liquid. Example is the preparation of Ammonia (NH_3) when iron (Fe) is used as catalyst, i.e. $N_2+3H_2 \rightarrow 2NH_3$.
Researchers have looked into the analysis of boundary layer flow with homogeneous-heterogeneous reaction because of its importance in the industry. Sravanthi et al. [22] recently examined the flow of a magnetite-water nanofluid in the presence of homogeneous and heterogeneous effects. Alzahrani et al. [23] investigated the influence of thermosolutal Marangoni convection and nanoparticle aggregation on Oldyroyd-B fluid with homogeneous and heterogeneous catalytic reactions. Sarojamma et al. [24] investigated the Cattaneo-Christov model in the homogeneous-heterogeneous autocatalytic chemical reaction of micropolar fluid. They observed that with diffusion ratios, the concentration of homogenous bulk fluid with microstructures drops, and the concentration of catalyst at the surface augments. Animasaun et al. [25] described a boundary layer generated on the surface with a changeable thickness of Erying-Powel liquid subject to equal diffusivity. Hayat et al. [26] considered the impacts of homogeneous and heterogeneous reactions on nanofluid flow over a surface with non-uniform thickness. Zhao et al. [27] utilized Buongiorno's model in the analysis of nanofluid flow characteristics in the presence of homogeneous and heterogeneous reactions.
Bioconvection is a pattern generation process that happens in the suspension of motile microorganisms when they swim in a given direction in response to certain stimuli Platt [28]. Because of density stratification, motile gyrotactic bacteria swim in large numbers to the upper layer of the fluid causing instability. Unlike motile gyrotactic microorganisms, the flow of nanoparticles immersed in the base fluid is induced by both thermophoresis and the Brownian motion mechanisms in the nanofluid Ramzan et al. [29]. The fact that the dispersion of nanoparticles in the base fluid can maintain the stability of the suspension in light of the instability caused by the motile microbes must also be emphasized. Bioconvection phenomena are essential in meteorological and medicinal applications such as pharmaceutical formulation, biopolymer synthesis, and microbial-enhanced oil recovery. Zhang et al. [30] examined the relevance of bioconvection flow with nanoparticles in the presence of Lorentz force. Rao et al. [31] investigated the bioconvection flow of nanofluid across an isothermal vertical cone with a chemical reaction. Sankad et al. [32] demonstrated boundary layer bioconvective flow with variable wall temperatures and thermal radiation effects. Parveen [33] investigated the effect of Brownian and thermophoresis motion on the peristaltic mechanism of conductive nanofluid flow via an asymmetric channel. Naganthran et al. [34] investigated scaling group analysis of bioconvective micropolar fluid in a porous regime.
To the best of the authors' knowledge, the hydromagnetic flow of nanofluid bioconvection with stratifications has been examined. However, researchers have not studied the impact of bioconvection flow of an electrically conducting Erying-Powel fluid containing nanoparticles in the presence of variable fluid characteristics and a quartic autocatalytic type of chemical reaction subjected to stratification over a surface with non-uniform thickness. Furthermore, the work addresses the role of thermophoresis and Brownian motion effects in nanofluid bioconvection flow. Two unique forms of stratification, thermal and motile microorganisms are integrated into the model which has a wide variety of applications in thermal energy storage systems, lakes, reservoirs, and the removal of residual pollutants. During the course of the inquiry, the current communication gives answers to the following questions:

- What effect does Darcy-Forchheimer have on velocity and temperature distributions?

- What impact does the Brownian motion parameter have on the homogeneous bulk fluid and heterogeneous catalyst surface concentration distributions?
- What impact does space-based internal heat generation parameter pose on the temperature distribution and concentration distribution of heterogeneous catalysts at the surface?
- What effect do the temperature-dependent viscous and thermal conductivity parameters have on velocity and temperature distributions, respectively?

2 Mathematical formulation of governing equation

The paper delves into the two-dimensional steady flow of bioconvective Erying-Powell fluid containing nanoparticles along the upper horizontal surface of a paraboloid of revolution. The Cauchy stress tensor in an Eyring-Powell fluid model studied by Ramzan et al. [35] is regulated by the relation

$$\tau_{ij} = \mu \frac{\partial u_i}{\partial x_j} + \frac{1}{\beta} \sinh^{-1}\left(\frac{1}{g}\frac{\partial u_i}{\partial x_j}\right), \tag{1}$$

The first term depicts the viscosity effect while the second term depicts the elastic part. Here μ is viscosity and β and g are the Eyring-Powell and rheological fluid parameters. Following Hayat et al. [36], Using Maclaurin series expansion of the hyperbolic sine is sufficient to describe the fluid,

$$\sinh^{-1}\left(\frac{1}{g}\frac{\partial u_i}{\partial x_j}\right) \cong \frac{1}{g}\frac{\partial u_i}{\partial x_j} - \frac{1}{6}\left(\frac{1}{g}\frac{\partial u_i}{\partial x_j}\right)^3, \quad \left|\frac{1}{g}\frac{\partial u_i}{\partial x_j}\right| \ll 1, \tag{2}$$

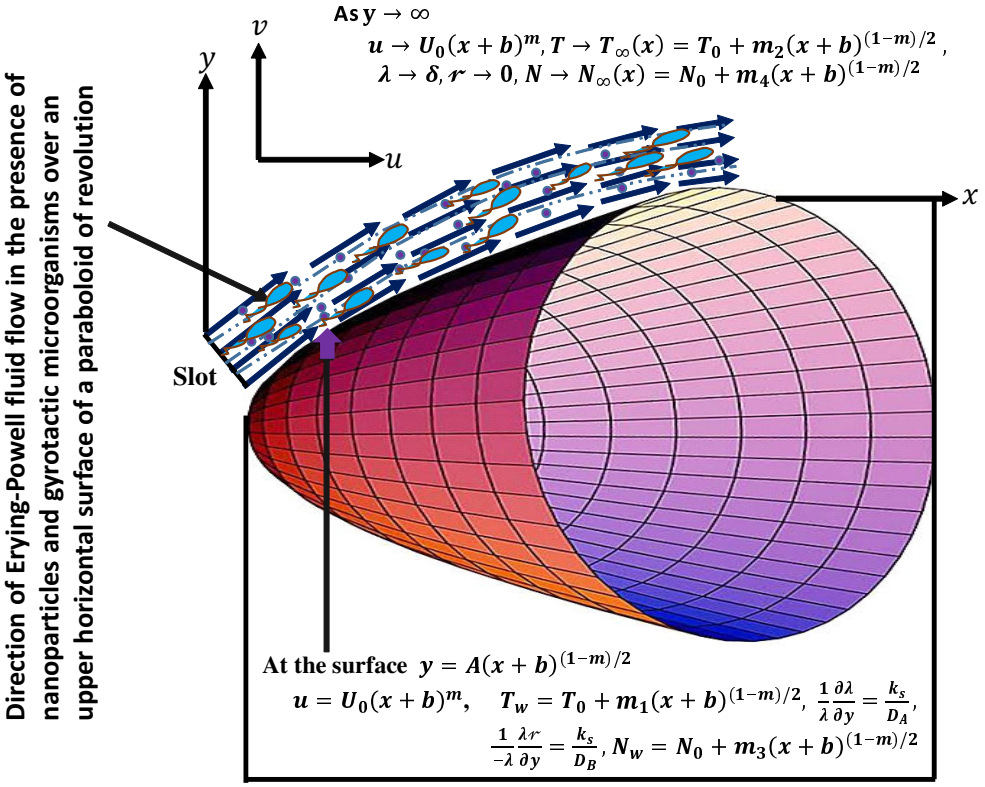

Figure 1. Geometry of Erying-Powell fluid flow over upper horizontal surface of a paraboloid of revolution

As the fluid flows along the upper horizontal surface of a paraboloid of revolution in a stratified domain, it is assumed that a quartic autocatalysis chemical reaction occurs between the reactant (bulk fluid) and concentrated catalyst on the wall. The chemical process is explained by Koriko and Animasaun [37] as a kind in which the homogeneous reaction is assumed to be by isothermal quartic autocatalytic kinetics and the heterogeneous reaction is considered to be by first-order kinetics. The concentrations of chemical species homogeneous bulk fluid (Eyring-Powell) A and heterogeneous catalyst B at the wall are denoted by λ and r, respectively. It is important to note that the Erying-Powell fluid flow over the surface with non-uniform thickness is assumed to occupy the domain $A(x+b)^{\frac{1-m}{2}} \leq y < \infty$, where $A \geq 0$. A and b are arbitrary constants associated with the thickness of the surface, m is velocity power index (see Fig. 1). In this study, m is less than 1. However, it is necessary to note that the flow of fluid along an upper horizontal surface of a paraboloid of revolution corresponds to $m < 1$(i.e$= 0.75$), Koriko et al. [25]. The upper horizontal surface of the paraboloid of revolution can be likened to the pointed upper surface of an aircraft, or the bonnet of a car. The fluid layers on an upper horizontal surface of the paraboloid of revolution are stretched with the velocity of $U_w = U_o(x+b)^m$, where U_o is the reference velocity. However, the velocities along $x, y-$ directions are $u(x,y)$ and $v(x,y)$, temperature is $T(x,y)$, concentrations of reactant A and reactant B are $\lambda(x,y)$ and $r(x,y)$ density of motile microorganisms is $N(x,y)$. To allow the microbes to live, water is assumed to be the base fluid. It is assumed that the suspension of nanoparticles inside the base fluid containing motile microorganisms will reduce bioconvection instability. Following Kuznetsov and Nield [38] and Rees et al. [39], microorganisms flux can be expressed as

$$\nabla . j = 0, \tag{3}$$

Following the idea of the homogeneous-heterogeneous reaction model proposed by Chaudhary and Merkin [40], Koriko et al. [41], Animasaun et al. [25], an isothermal quartic autocatalytic reaction in the homogeneous case is expressed as

$$A + 3B \rightarrow 4B, \tag{4}$$

where the chemical reaction rate $= k_h \lambda r^3$ while the chemical reaction on the surface of the catalyst is expressed as

$$A \rightarrow B, \tag{5}$$

where the chemical reaction rate $= k_s \lambda$. The concentrations of chemical reactants A and B are λ and r. Coefficient of chemical reaction rate are k_h and k_s. Following Kuznetsov [42], microorganisms flux j relating to the concentration of the homogeneous chemical reactant A is expressed as

$$j = Nv + N\widetilde{v} - D_m \nabla N, \qquad \widetilde{v} = \left(\frac{bW_c}{\Delta\lambda}\right)\nabla\lambda\,, \tag{6}$$

in which v is the velocity vector of the flow, $\widetilde{v}$ is the average swimming velocity vector of oxytactic microorganism, b is the chemotaxis contant, W_c is the maximum cell swimming speed and D_m is the diffusivity of microorganisms. With all the aforementioned assumptions, the governing equation that is suitable to analyze the bioconvective flow of Erying-Powell fluid with nanoparticles following the formulations of Refs. [25, 31, 36, 41] is presented as continuity

equation:

$$\frac{\partial u}{\partial x} + \frac{\partial v}{\partial y} = 0. \tag{7}$$

The momentum equation with the non-Newtonian fluid term and the magnetic field term takes the form

$$u\frac{\partial u}{\partial x} + v\frac{\partial u}{\partial y} = \frac{1}{\rho_f}\frac{\partial}{\partial y}\left[\left(\mu_f(T) + \frac{1}{\beta_j C}\right)\frac{\partial u}{\partial y}\right] - \frac{1}{2\beta_j C^3 \rho}\frac{\partial u}{\partial y}\frac{\partial u}{\partial y}\frac{\partial^2 u}{\partial y^2} - \frac{\sigma_f {B_o}^2 u}{\rho_f} - \frac{\mu(T)}{\rho}\frac{1}{k}u - \frac{b^*}{k}u^2. \tag{8}$$

The energy equation in which the exponential space-based heat generation, stratification, thermophoresis, and Brownian motion are incorporated and take the form

$$u\frac{\partial T}{\partial x} + v\frac{\partial T}{\partial y} = \frac{1}{(\rho C_p)_f}\frac{\partial}{\partial y}\left(\kappa_f(T)\frac{\partial T}{\partial y}\right) + \tau\left[D_B\frac{\partial T}{\partial y}\frac{\partial \lambda}{\partial y} + \frac{D_T}{T_\infty}\left(\frac{\partial T}{\partial y}\right)^2\right] + \frac{Q_o(T_w - T_0)}{(\rho C_p)_f} Exp^{-ny\sqrt{\frac{c(m+1)}{2\vartheta}}(x+b)^{\frac{m-1}{2}}}. \tag{9}$$

The effect of thermophoresis and the homogeneous-heterogeneous reaction model on reactant A and B concentrations is given as

$$u\frac{\partial \lambda}{\partial x} + v\frac{\partial \lambda}{\partial y} = D_A\frac{\partial^2 \lambda}{\partial y^2} - \frac{D_T}{T_\infty}\frac{\partial^2 T}{\partial y^2} - k_h \lambda r^3, \tag{10}$$

$$u\frac{\partial r}{\partial x} + v\frac{\partial r}{\partial y} = D_B\frac{\partial^2 r}{\partial y^2} + \frac{D_T}{T_\infty}\frac{\partial^2 T}{\partial y^2} + k_h \lambda r^3. \tag{11}$$

Density of gyrotactic microorganisms equation in the homogeneous bulk fluid is presented as

$$u\frac{\partial N}{\partial x} + v\frac{\partial N}{\partial y} + \frac{bW_c}{\Delta\lambda}\left[\frac{\partial}{\partial y}\left(N\frac{\partial \lambda}{\partial y}\right)\right] = D_n\frac{\partial^2 N}{\partial y^2}. \tag{12}$$

The associated boundary conditions that connect chemical changes of the reactants A and B at the surface, the thermal and motile microorganisms stratifications are expressed as

$$u = U_o(x+b)^m,\ v = 0,\ T = T_w,\ \frac{1}{\lambda}\frac{\partial \lambda}{\partial y} = \frac{k_s}{D_A},\ \frac{1}{-\lambda}\frac{\partial r}{\partial y} = \frac{k_s}{D_B}, N = N_w \text{ at } y = A(x+b)^{\frac{1-m}{2}}, \tag{13}$$

$$u \to 0, \quad T \to T_\infty, \quad \lambda \to \delta, \quad r \to 0 \quad N \to N_\infty \quad \text{as} \quad y \to \infty, \tag{14}$$

where β_j is the Erying-Powell fluid parameter κ is thermal conductivity, σ is the fluid electrical conductivity, ρ is the fluid density, B_o is the magnetic field strength, T is the fluid temperature, Q_o

is the heat generation/absorption, ρC_p is the heat capacity of the fluid.
The temperature-dependent viscosity mathematical model was developed using Batchelor's experimental data [43], as well as the mathematical model of temperature-dependent thermal conductivity of Charraudeau [44] and Yook et al. [45] as;

$$\mu_f(T) = \mu_f^*[1 + b(T_w - T)] \quad \text{and} \quad \kappa_f(T) = \kappa_f^*[1 + \delta(T - T_\infty)]. \tag{15}$$

Following [46–48], it is essential to indicate how stratification is incorporated into the energy and concentration equations as we express the thermal stratification at the wall (T_w) and solutal stratification at the wall (C_w) and the free stream temperature and concentration $(T_\infty,\ C_\infty)$ as

$$\begin{aligned} T_w - T_0 &= m_1(x+b)^{\frac{1-m}{2}} \quad \text{and} \quad T_\infty - T_0 = m_2(x+b)^{\frac{1-m}{2}}, \\ N_w - N_0 &= m_3(x+b)^{\frac{1-m}{2}} \quad \text{and} \quad N_\infty - N_0 = m_4(x+b)^{\frac{1-m}{2}}, \end{aligned} \tag{16}$$

where T_0 is the reference temperature, it is worth noting that stratification occurs for all points of x on the wall at $y = A(x+b)^{\frac{1-m}{2}}$ and also for all points of x at the ambient as $y \to \infty$.

The essential physical quantities of engineering in the Erying-Powell are expressed as in Animasaun et al. [25]

$$\begin{aligned} C_f &= \left[\left(\frac{\mu_f(T)}{\rho_f} + \frac{1}{\beta_j C}\right)\frac{\partial u}{\partial y} - \frac{2}{m+1}\frac{1}{\beta_j C^3}\left(\frac{\partial u}{\partial y}\right)^3\right]_{y=A(x+b)^{\frac{1-m}{2}}}, \\ Nu_x &= \frac{(x+b)\,q_w}{\kappa(T_w(x) - T_0)\left(\frac{m+1}{2}\right)^{\frac{1}{2}}}, \quad where \ \ q_w = -\kappa\frac{\partial T}{\partial y}\bigg|_{y=A(x+b)^{\frac{1-m}{2}}}. \end{aligned} \tag{17}$$

For the sake of transformation, the following similar transformations can be expressed as

$$u = \frac{\partial \psi}{\partial y},\ v = -\frac{\partial \psi}{\partial x},\ \eta = y\left(\frac{U_o(m+1)}{2\vartheta}\right)^{1/2}(x+b)^{\frac{m-1}{2}},\ \psi = \left(\frac{2\vartheta U_o}{m+1}\right)^{1/2}(x+b)^{\frac{m+1}{2}} f(\eta),$$

$$\theta(\eta) = \frac{T - T_\infty}{T_w - T_0}, \qquad \frac{\lambda}{\delta} = q(\eta), \quad \frac{r}{\delta} = s(\eta), \qquad \omega(\eta) = \frac{N - N_\infty}{N_w - N_0}. \tag{18}$$

Using the similar transformation, stream function $\psi(x,\ y)$ satisfies the continuity equation, the governing partial differential equations (8)-(12) together with the boundary conditions (13)-(14) are converted to the system of nonlinear differential equations expressed as

$$\begin{aligned} &\left([1 + (1 - \theta(\eta))\,\xi] + \varsigma - \varsigma\mathcal{H}\frac{(m+1)}{2}\frac{d^2f}{d\eta^2}\frac{d^2f}{d\eta^2}\right)\frac{d^3f}{d\eta^3} - \xi\frac{d^2f}{d\eta^2}\frac{d\theta}{d\eta} - \frac{2m}{m+1}\frac{df}{d\eta}\frac{df}{d\eta} \\ &+ f(\eta)\frac{d^2f}{d\eta^2} - \frac{2}{m+1}M\frac{df}{d\eta} - \frac{2}{m+1}[1 + (1-\theta)\,\xi]\,P_s\frac{df}{d\eta} - \frac{2}{m+1}F_sD_a^{-1}\frac{df}{d\eta}\frac{df}{d\eta} = 0, \end{aligned} \tag{19}$$

$$[1+\theta(\eta)\varepsilon]\frac{d^2\theta}{d\eta^2}-\frac{2}{m+1}P_r\theta(\eta)\frac{df}{d\eta}-\frac{2}{m+1}S_tP_r\frac{df}{d\eta}+P_rf(\eta)\frac{d\theta}{d\eta}+\varepsilon\frac{d\theta}{d\eta}\frac{d\theta}{d\eta}+P_rN_b\frac{d\theta}{d\eta}\frac{dq}{d\eta}$$
$$+P_rN_t\frac{d\theta}{d\eta}\frac{d\theta}{d\eta}+\frac{2}{m+1}\zeta P_re^{-n\eta}=0, \tag{20}$$

$$\frac{d^2q}{d\eta^2}+S_{cA}f(\eta)\frac{dq}{d\eta}-\frac{N_t}{N_b}\frac{d^2\theta}{d\eta^2}-\frac{2}{m+1}S_{cA}\mathcal{R}q(\eta)s^3(\eta)=0, \tag{21}$$

$$\gamma\frac{d^2s}{d\eta^2}+S_{cB}f(\eta)\frac{ds}{d\eta}+\frac{N_t}{N_b}\frac{d^2\theta}{d\eta^2}+\frac{2}{m+1}S_{cB}\mathcal{R}q(\eta)s^3(\eta)=0, \tag{22}$$

$$\frac{d^2\omega}{d\eta^2}-\frac{2}{m+1}S_{cm}\omega(\eta)\frac{df}{d\eta}-\frac{2}{m+1}S_{cm}S_g\frac{df}{d\eta}+S_{cm}f(\eta)\frac{d\omega}{d\eta}-P_e\omega\frac{d^2q}{d\eta^2}-P_e\frac{dq}{d\eta}\frac{d\omega}{d\eta}$$
$$-P_e\frac{d^2q}{d\eta^2}-P_eS_g\frac{d^2q}{d\eta^2}=0. \tag{23}$$

It is important to note that at the surface $y=A(x+b)^{\frac{1-m}{2}}$, the minimum value of y which corresponds to minimum value of the similarity variable

$$\eta=\sqrt{\frac{U_o(m+1)}{2\vartheta}}=\Im. \tag{24}$$

Then the boundary conditions become

$$f(\Im)=\Im\frac{1-m}{1+m},\quad \frac{df}{d\Im}=1,\quad \theta(\Im)=1-S_t,\quad \frac{1}{\mathcal{J}}\frac{dq}{d\Im}=q(\Im),$$
$$\frac{\gamma}{\mathcal{J}}\frac{ds}{d\Im}=-q(\Im),\quad \omega(\Im)=1-S_g\quad at\ \Im=\eta, \tag{25}$$

$$\frac{df}{d\Im}\to 0,\ \theta(\Im)\to 0,\ q(\Im)\to 1,\ s(\Im)\to 0,\ \omega(\Im)\to 0\quad as\ \eta\to\Im. \tag{26}$$

The transformed governing equations (19)-(23) are dependent on η while the boundary conditions are dependent on $\Im$. It is therefore, necessary to change the domain from $[\Im,\infty]$ to $[0,\infty]$ which is done by defining $F(\aleph)=F(\eta-\Im)=f(\eta)$, $\Theta(\aleph)=\Theta(\eta-\Im)=\theta(\eta)$, $\mathrm{Q}(\aleph)=\mathrm{Q}(\eta-\Im)=q(\eta)$, $\mathrm{S}(\aleph)=\mathrm{S}(\eta-\Im)=s(\eta)$ and $\mathrm{W}(\aleph)=\mathrm{W}(\eta-\Im)=w(\eta)$. The dimensionless governing equations (19)-(23) take a new form

$$\left([1+(1-\Theta(\aleph))\xi]+\varsigma-\varsigma\mathcal{H}\frac{(m+1)}{2}\frac{d^2F}{d\aleph^2}\frac{d^2F}{d\aleph^2}\right)\frac{d^3F}{d\aleph^3}-\xi\frac{d^2F}{d\aleph^2}\frac{d\Theta}{d\aleph}$$
$$-\frac{2m}{m+1}\frac{dF}{d\aleph}\frac{dF}{d\aleph}+F(\aleph)\frac{d^2F}{d\aleph^2}-\frac{2}{m+1}M\frac{dF}{d\aleph}-\frac{2}{m+1}[1+(1-\Theta)\xi]P_s\frac{dF}{d\aleph} \tag{27}$$
$$-\frac{2}{m+1}F_sD_a^{-1}\frac{dF}{d\aleph}\frac{dF}{d\aleph}=0,$$

$$[1+\Theta(\aleph)\varepsilon]\frac{d^2\Theta}{d\aleph^2}-\frac{2}{m+1}P_r\Theta(\aleph)\frac{df}{d\aleph}-\frac{2}{m+1}S_tP_r\frac{dF}{d\aleph}+P_rF(\aleph)\frac{d\Theta}{d\aleph}$$
$$+\varepsilon\frac{d\Theta}{d\aleph}\frac{d\Theta}{d\aleph}+P_rN_b\frac{d\Theta}{d\aleph}\frac{dQ}{d\aleph}+P_rN_t\frac{d\Theta}{d\aleph}\frac{d\Theta}{d\aleph}+\frac{2}{m+1}\zeta P_re^{-n\eta}=0, \tag{28}$$

$$\frac{d^2Q}{d\aleph^2}+S_{cA}F(\aleph)\frac{dQ}{d\aleph}-\frac{N_t}{N_b}\frac{d^2\Theta}{d\aleph^2}-\frac{2}{m+1}S_{cA}\mathcal{R}Q(\aleph)S^3(\aleph)=0, \tag{29}$$

$$\gamma\frac{d^2S}{d\aleph^2}+S_{cB}F(\aleph)\frac{dS}{d\aleph}+\frac{N_t}{N_b}\frac{d^2\Theta}{d\aleph^2}+\frac{2}{m+1}S_{cB}\mathcal{R}q(\aleph)S^3(\aleph)=0, \tag{30}$$

$$\frac{d^2W}{d\eta^2}-\frac{2}{m+1}S_{cm}W(\aleph)\frac{dF}{d\aleph}-\frac{2}{m+1}S_{cm}S_g\frac{dF}{d\aleph}+S_{cm}F(\aleph)\frac{dW}{d\aleph}-P_eW\frac{d^2Q}{d\aleph^2}$$
$$-P_e\frac{dQ}{d\aleph}\frac{dW}{d\aleph}-P_e\beth\frac{d^2Q}{d\aleph^2}-P_eS_g\frac{d^2Q}{d\aleph^2}=0, \tag{31}$$

The boundary conditions become

$$F(\aleph)=\Im\frac{1-m}{1+m},\quad \frac{dF}{d\aleph}=1,\quad \Theta(\aleph)=1-S_t,\quad \frac{1}{\mathcal{J}}\frac{dQ}{d\aleph}=Q(\aleph)$$
$$\frac{\gamma}{\mathcal{J}}\frac{dS}{d\aleph}=-Q(\aleph),\qquad W(\aleph)=1-S_g\quad at\quad \aleph=0, \tag{32}$$

$$\frac{dF}{d\aleph}\to 0,\Theta(\aleph)\to 0,\ Q(\aleph)\to 1,\ S(\aleph)\to 0,\ W(\aleph)\to 0\quad as\quad \aleph\to\infty. \tag{33}$$

Through the usage of the similarity variables in Eqs. (17), Eqs. (18) can be non-dimensionalized to obtain

$$Re_x^{\frac{1}{2}}C_{f=}\left[[(1+(\xi-\xi\Theta))+\varsigma]\frac{d^2F}{d\aleph^2}-\xi\frac{dF}{d\aleph}\frac{d\Theta}{d\aleph}-\varsigma\mathcal{H}\frac{d^2F}{d\aleph^2}\frac{d^2F}{d\aleph^2}\frac{d^2F}{d\aleph^2}\right]_{\aleph=0},$$
$$Re_x^{-\frac{1}{2}}Nu_x=-\frac{\mathrm{d}\Theta}{d\aleph}\bigg|_{\aleph=0}, \tag{34}$$

where Re_x is the local Reynolds number.

Erying-Powell fluid parameters are $\varsigma=\frac{1}{\beta_jC\mu}$, $\mathcal{H}=\frac{U_0^3(x+b)^{3m-1}}{2C^2\vartheta}$, temperature-dependent viscous parameter $\xi=\varpi(T_w-T_0)$, magnetic parameter $\frac{\sigma{B_o}^2}{\rho U_0}(x+b)^{-m+1}$, temperature-dependent thermal conductivity parameter $\varepsilon=\delta(T_w-T_0)$, thermophoresis parameter $N_t=\frac{\tau(T_w-T_0)}{\alpha}\frac{D_T}{T_\infty}$, Brownian motion parameter $N_b=\frac{\tau D_A\delta}{\alpha}$, thermal stratification $S_t=\frac{m_2}{m_1}$, space-dependent internal heat source parameter $\zeta=\frac{Q_o}{\rho C_pc(x+b)^{m-1}}$, n is the intensity of internal heat generation parameter, Schmidt number for reactant A $S_{cA=}\frac{\vartheta}{D_A}$, Schmidt number for reactant B $S_{cB}=\frac{\vartheta}{D_B}$, homogeneous reaction parameter $\mathcal{R}=\frac{k_h\delta^3}{U_0(x+b)^{m-1}}$, Porosity parameter $P_s=\frac{\vartheta}{kU_o}(x+b)^{1-m}$, local Forchheimer pa-

rameter $F_s = \frac{b^*}{(x+b)}$, local Darcy parameter $D_a = \frac{k}{(x+b)^2}$, Gyrotactic microorganisms concentration difference parameter $\beth = \frac{N_o}{N_w - N_0}$, Schmidt number for diffusing motile microorganisms $S_{cm} = \frac{\vartheta}{D_n}$, Peclet number $P_e = \frac{bW_c}{\mathrm{D_n}\acute{\lambda}}$, gyrotactic microorganisms density stratification parameter $S_g = \frac{m_4}{m_3}$, heterogeneous reaction parameter $\mathcal{J} = \frac{k_s}{D_A\sqrt{\frac{U_0(m+1)}{2\vartheta}}\,(x+b)^{\frac{m-1}{2}}}$, ratio of diffusion coefficient $\gamma = \frac{D_A}{D_B}$.

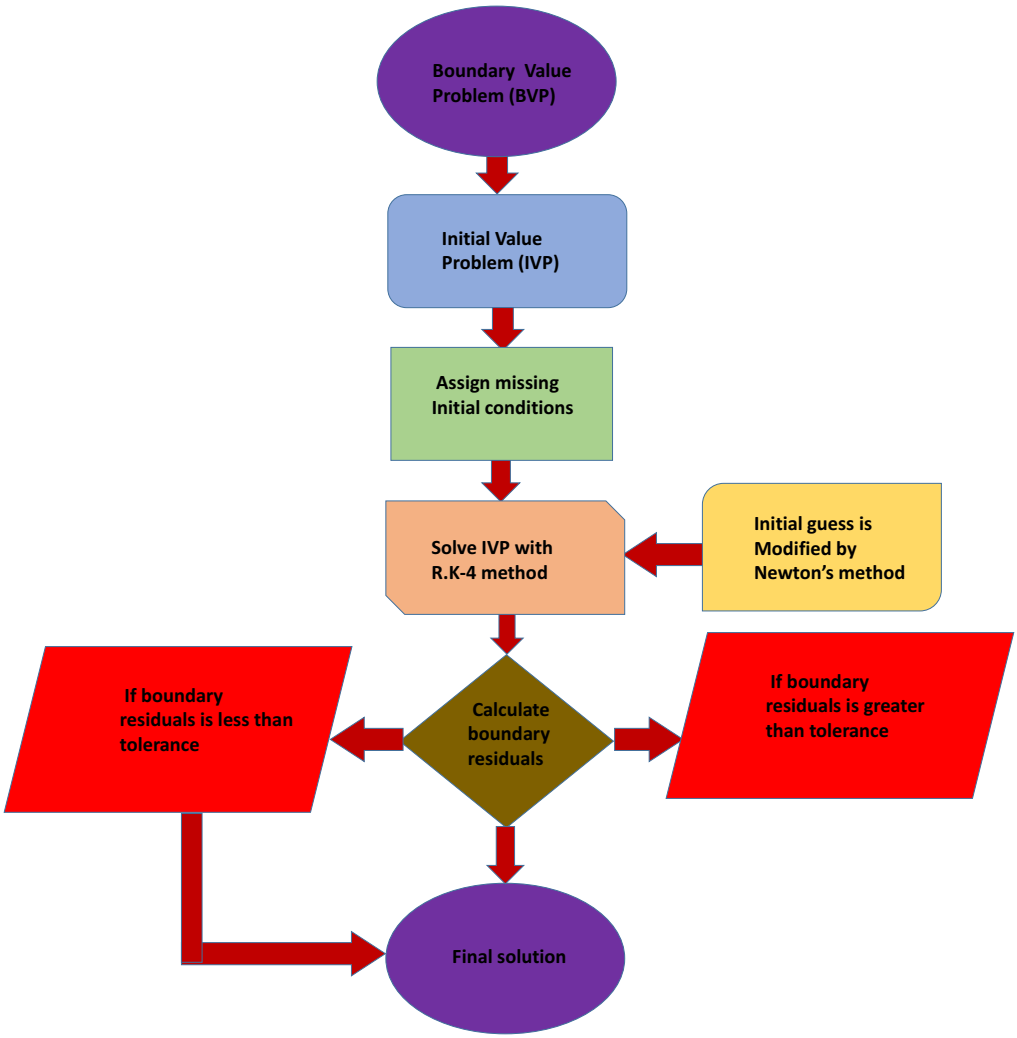

Figure 2. Flow chart of the problem

3 Numerical solution: procedure of the shooting technique

The procedure for obtaining the numerical solutions with the aid of $RK-4$ alongside with shooting technique is expressed in Fig. 2. To be able to carry out the operation of the shooting technique, the system of dimensionless Eqs. (27)-(31) is reduced to the following system of first-order ordinary differential equations;

$$F = y_1,$$

$$\frac{dF}{d\aleph} = y_2,$$

$$\frac{d^2F}{d\aleph^2} = y_3,$$

$$\frac{d^3f}{d\aleph^3} = y_3' = \frac{\xi y_3 y_5 + \frac{2m}{m+1} y_2 y_2 - y_1 y_3 + \frac{2}{m+1} M y_2 + \frac{2}{m+1} P_s \left[1 + \left(1 - y_4\right) \xi\right] y_2 + \frac{2}{m+1} F_s D_a^{-1} y_2 y_2}{\left(\left[1 + (1 - y_4)\, \xi\right] + \varsigma - \varsigma \mathcal{H} \frac{(m+1)}{2} y_3 y_3\right)},$$

$$\Theta = y_4,$$

$$\frac{d\Theta}{d\aleph} = y_5,$$

$$\frac{d^2\Theta}{d\aleph^2} = y_5' = \frac{\left(\frac{2}{m+1} P_r y_4 y_2 + \frac{2}{m+1} S_t P_r y_2 - P_r y_1 y_5 - \varepsilon y_5 y_5 - P_r N_b y_5 y_7 - P_r N_t y_5 y_5 - \frac{2}{m+1} \zeta P_r \mathrm{e}^{-n\aleph}\right)}{[1 + y_4 \varepsilon]}$$

$$Q = y_6,$$

$$\frac{dQ}{d\aleph} = y_7,$$

$$\begin{aligned}
&\frac{d^2Q}{d\aleph} = y_7' \\
&= \frac{N_t}{N_b} \left(\frac{\left(\frac{2}{m+1} P_r y_4 y_2 + \frac{2}{m+1} S_t P_r y_2 - P_r y_1 y_5 - \varepsilon y_5 y_5 - P_r N_b y_5 y_7 - P_r N_t y_5 y_5 - \frac{2}{m+1} \zeta P_r \mathrm{e}^{-n\aleph}\right)}{[1 + y_4 \varepsilon]} \right) \\
&- S_{cA} y_1 y_7 + \frac{2}{m+1} S_{cA} \mathcal{R} y_6 y_8 y_8 y_8,
\end{aligned}$$

$$S = y_8,$$

$$\frac{dS}{d\aleph} = y_9,$$

$$\frac{d^2S}{d\aleph} = y_9' = \frac{\left(\frac{N_t}{N_b} \frac{dy_5}{d\eta} - S_{cB} y_1 y_9 - \frac{2}{m+1} S_{cB} \mathcal{R} y_6 y_8 y_8 y_8\right)}{\gamma}$$

$$W = y_{10},$$

$$\frac{dW}{d\aleph} = y_{11},$$

$$\frac{d^2W}{d\aleph^2} = y'_{11} = \frac{2}{m+1}S_{cm}y_{10}y_2 + \frac{2}{m+1}S_{cm}S_g y_2 - S_{cm}y_1 y_{11} + \frac{dy_7}{d\eta}\left(P_e y_{10} + P_e S_g + P_e \beth\right) + P_e y_7 y_{11}, \tag{35}$$

Subject to boundary conditions:

$$y_1(0) = \Im\frac{1-m}{1+m}, \quad y_2(0) = 1, \quad y_4(0) = 1 - S_t,$$
$$\frac{1}{\mathcal{J}}y_7(0) = y_6(0), \quad \frac{\gamma}{\mathcal{J}}y_9(0) = -y_6(0), \quad y_{10}(0) = 1 - S_g \quad at\ \aleph = 0, \tag{36}$$

$$y_2(0) \to 0,\ y_4(0) \to 0, y_6(0) \to 1, y_8(0) \to 0,\ y_{10}(0) \to 0 \quad as\ \aleph \to \infty.$$

Initial approximations were selected and Eqs. (35) and (36) are integrated numerically as an initial value problem with the tolerance level of 10^{-6} and the boundary condition at a finite point considered as $\aleph = 6$.

4 Analysis of results and discussion

The values of pertinent parameters have been carefully selected during the process of computations as $\varsigma = \mathcal{H} = 0.1, m = 0.75,\ \Im = 0.25,\ S_t = S_g = 0.1, P_s = F_s = D_a = 0.3,\ P_r = 1.0,\ P_e = 1.0$ so as to be able to properly observe the impacts on fluid flow within the boundary layer. Table 1 depicts the numerical values of physical quantities of engineering interest expressed in Eq. (34). Likewise, Table 2 shows the validation of results with two different techniques. It is noticed that there is reasonable agreement with both *shooting technique* and *Bvp4c*. The effect of Darcy-Forchheimer

Table 1. Variation in local skin friction coefficients, local heat transfer rate with various parameters when $m = 0.25,\ \varsigma = \mathcal{H} = 0.1, \Im = 0.25,\ S_t = S_g = 0.1,\ P_e = 1.0,\ \zeta = 0.4,\ L_e = 0.1,\ \gamma = 1.0,\ \mathcal{R} = 0.2, \mathcal{J} = 0.1$

F_s	D_a	ξ	ε	M	P_r	N_t	N_b	$C_f Re_x^{1/2}$	$Nu_x\ Re_x^{-\frac{1}{2}}$
0.1	0.1	0.3	0.4	0.5	1.0	0.1	0.1	−3.68398	−0.335823
0.3								−4.89971	−0.060089
	0.4							−3.501747	−0.382399
	0.6							−3.30933	−0.433187
		0.4						−3.30171	−0.438490
		0.7						−3.280692	−0.454088
			0.5					−3.279882	−0.430422
			0.8					−3.278111	−0.374863
				0.6				−3.385541	−0.321764
				1.0				−3.785906	−0.143243
					1.2			−3.778422	−0.146725
					2.0			−3.754425	−0.187570
						0.3		−3.733414	−0.067809
						0.6		−3.686839	0.214499
							0.2	−3.714673	0.051744
							0.5	−3.778341	−0.298297

Table 2. Validation of results and variations in $Nu_x\ Re_x^{-\frac{1}{2}}$ when $m = 0.25,\ \varsigma = \mathcal{H} = 0.1, \Im = 0.25,\ S_t = S_g = 0.1,\ P_r = 2.0,\ P_e = 1.0,\ N_t = 0.1,$ $\xi = \varepsilon = 0.3,\ \zeta = 0.4,\ L_e = 0.1,\ \gamma = 1.0,\ \mathcal{R} = 0.2, \mathcal{J} = 0.1,\ P_s = F_s = D_a = 0.3$

M	$Nu_x\ Re_x^{-\frac{1}{2}}$ (Shooting Technique)	$Nu_x\ Re_x^{-\frac{1}{2}}$ (Bvp4c)
0.1	−1.097833	−1.097831
0.4	−0.732341	−0.732340
0.5	−0.399743	−0.399742
0.7	−0.102830	−0.102829

parameter $(F_s,\ D_a)$ is revealed in Figs. 3(a) and 3(b), it is revealed in Fig. 3(a) that incremental values of $F_s,\ D_a$ cause a slight decline in the velocity distribution while an enhancement is noticed in the temperature distribution in Fig. 3(b).

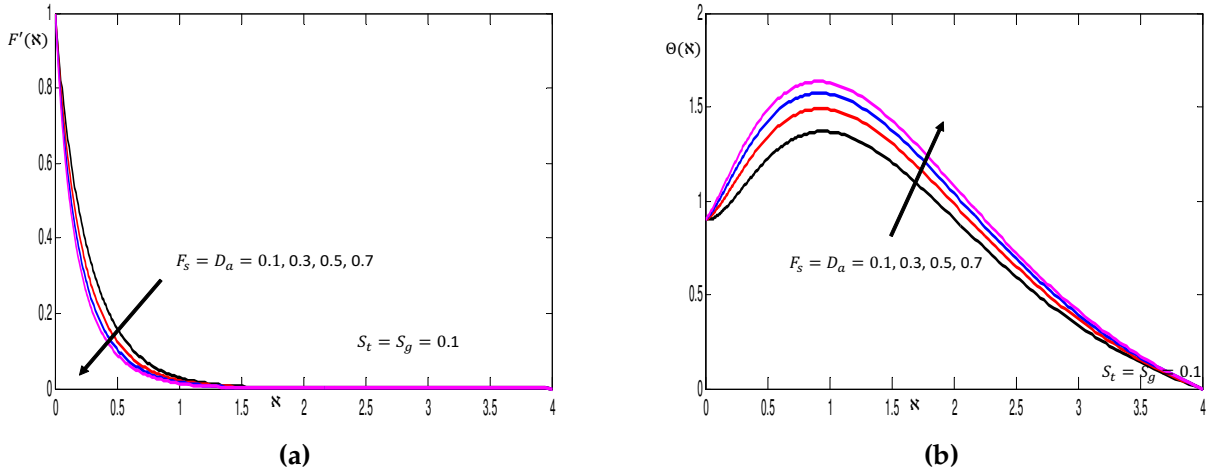

Figure 3. The changes in the **(a)** contribution of F_s, D_a on velocity distribution and **(b)** contribution of F_s, D_a on temperature distribution

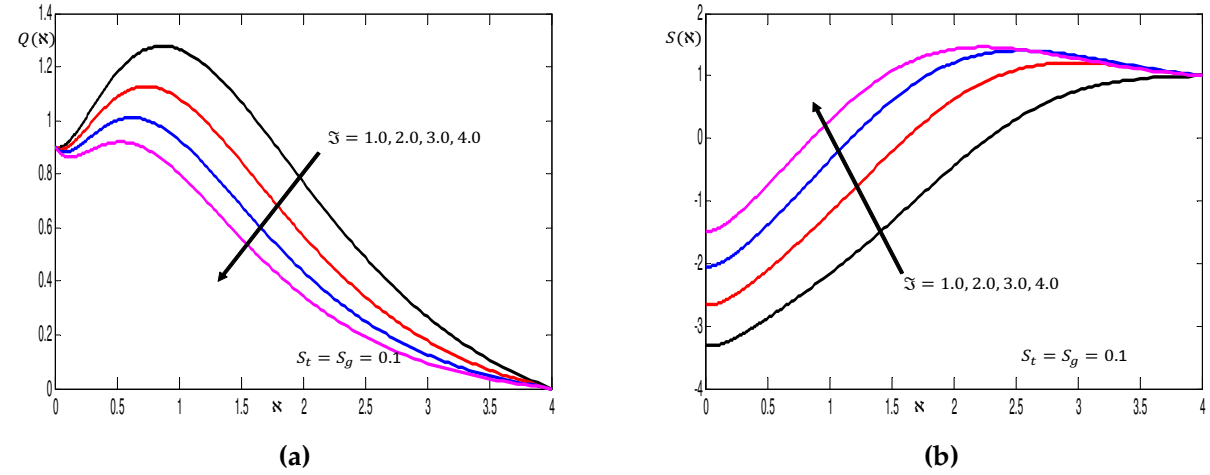

Figure 4. The changes in the **(a)** contribution of $\Im$ on concentration distribution of homogeneous bulk fluid and **(b)** contribution of $\Im$ on concentration distribution of heterogeneous catalysts at the surface

It is observed in Fig. 4(a) that there is a diminution in the concentration distribution of homogeneous bulk fluid with increased thickness parameter $\Im$, while in Fig. 4(b) augmentation in the concentration distribution of heterogeneous catalyst at the surface is noticed as thickness parameter increases. In Figs. 5(a) and 5(b) incremental values of space-based internal heat generation parameter ζ correspond to augmentation of both the temperature distribution and concentration distribution of heterogeneous catalyst at the surface, respectively. Physically, this observation is due to the fact that there is a provision of sufficient heat energy required to break down the strong intermolecular bond binding the molecules of the particles of the fluid together which permits the free flow of the fluid over the upper horizontal surface of a paraboloid of revolution.

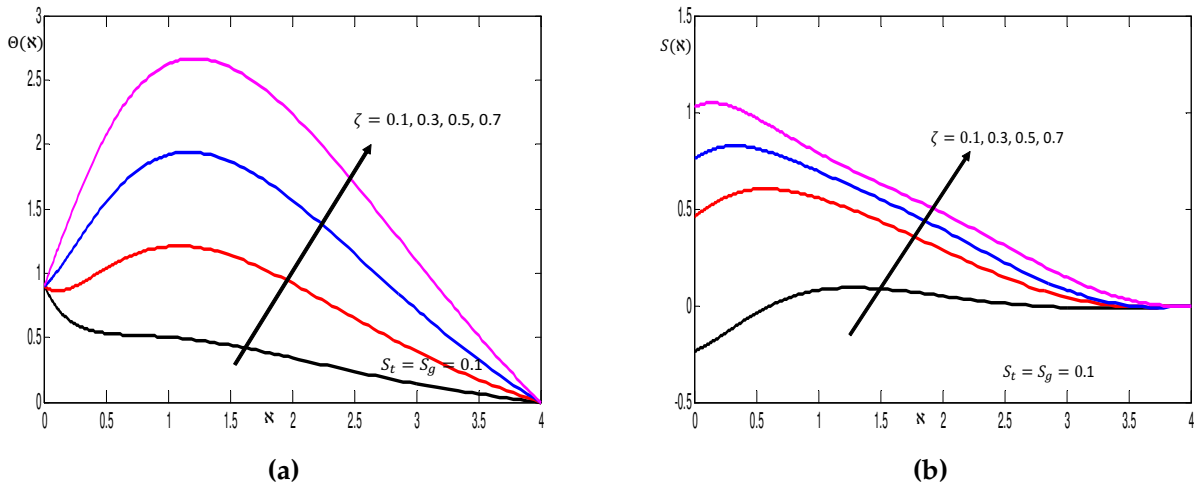

Figure 5. The changes in the **(a)** contribution of ζ on temperature distribution and **(b)** contribution of ζ on concentration distribution of heterogeneous catalysts at the surface

The impact of the thermal stratification parameter S_t is observed in Figs. 6(a),6(b),7(a). In Fig. 6(a), it is observed that incremental values of S_t lead to a diminution of the temperature distribution, while an enhancement in the concentration of reactant is noticed in Fig. 6(b).

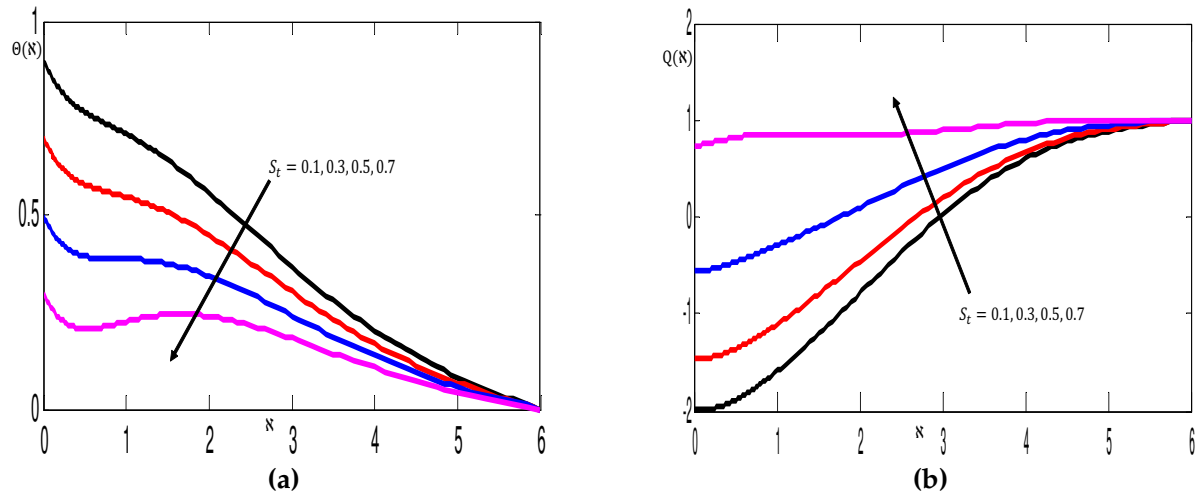

Figure 6. The changes in the **(a)** contribution of S_t on temperature distribution and **(b)** contribution of S_t on concentration distribution of homogeneous bulk fluid

It is visualized in Fig. 7(a) that increasing S_t corresponds to a decline in the bioconvection distribution, while a different behaviour is noticed in Fig. 7(b) in the sense that, as S_g is raised, the bioconvection distribution diminishes within the domain $0 \leq \aleph \leq 2.4$ and thereafter, an augmentation is noticed within the domain $2.4 \leq \aleph \leq 6.0$.

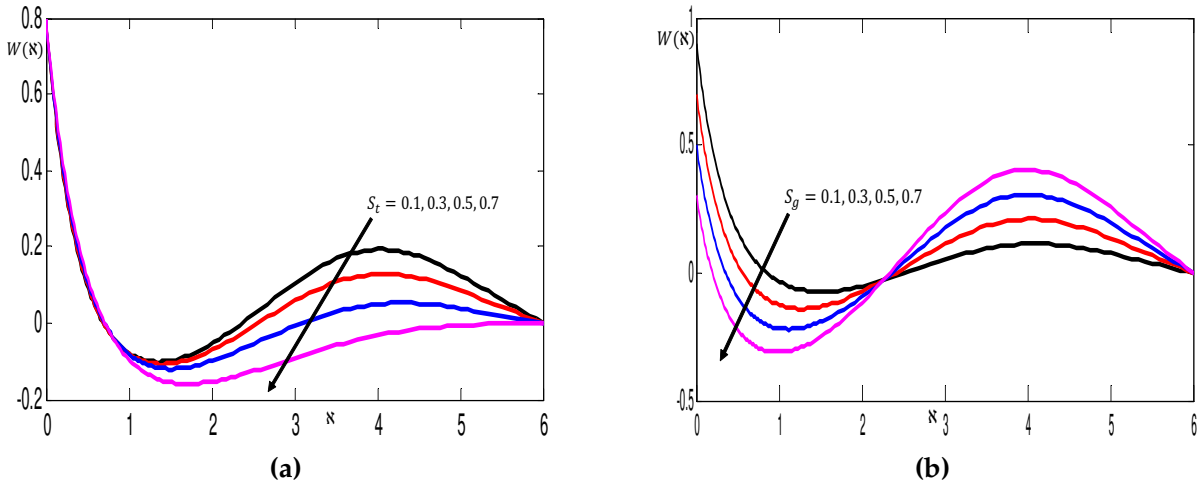

Figure 7. The changes in the **(a)** contribution of S_t bioconvection distribution and **(b)** contribution of S_g bioconvection distribution

The influence of material parameter ς is reflected in Figs. 8-10 when $S_t = S_g = 0.1$ (that is, at the hypolimnion layer of stratification). It is observed in Fig. 8(a) that the velocity of the fluid is enhanced as it flows over the upper horizontal surface of the paraboloid of revolution. The observed trend is due to the fact that $\varsigma = \frac{1}{\beta_j C\mu}$ means if ς increases, automatically the viscosity of the Erying-Powell fluid is subsided, thereby boosting the motion of the fluid across the upper horizontal surface of the paraboloid of revolution. An opposite effect is noticed in temperature distribution in Fig. 8(b) as ς increases.

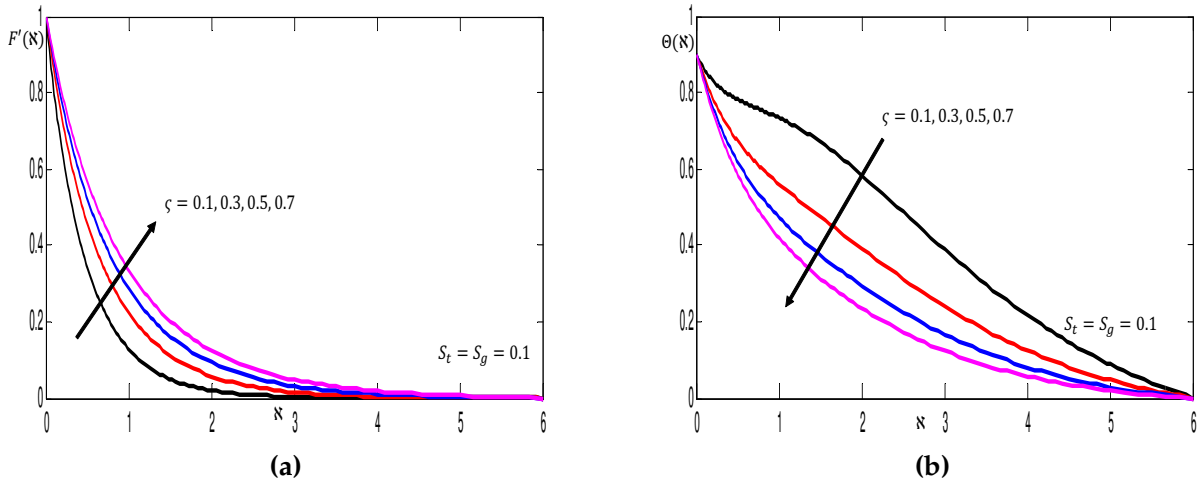

Figure 8. The changes in the **(a)** contribution of ς on velocity distribution and **(b)** contribution of ς on temperature distribution

Fig. 9(a) unravels the contribution of ς on the concentration of reactant A that is also known as the homogeneous bulk fluid. It is deduced that the magnitude of ς leads to a significant enhancement of the concentration of reactant A at the initial stage of the stratification, meanwhile, with the same magnitude of ς large diminution is noticed in the concentration of reactant B and bioconvection distribution.

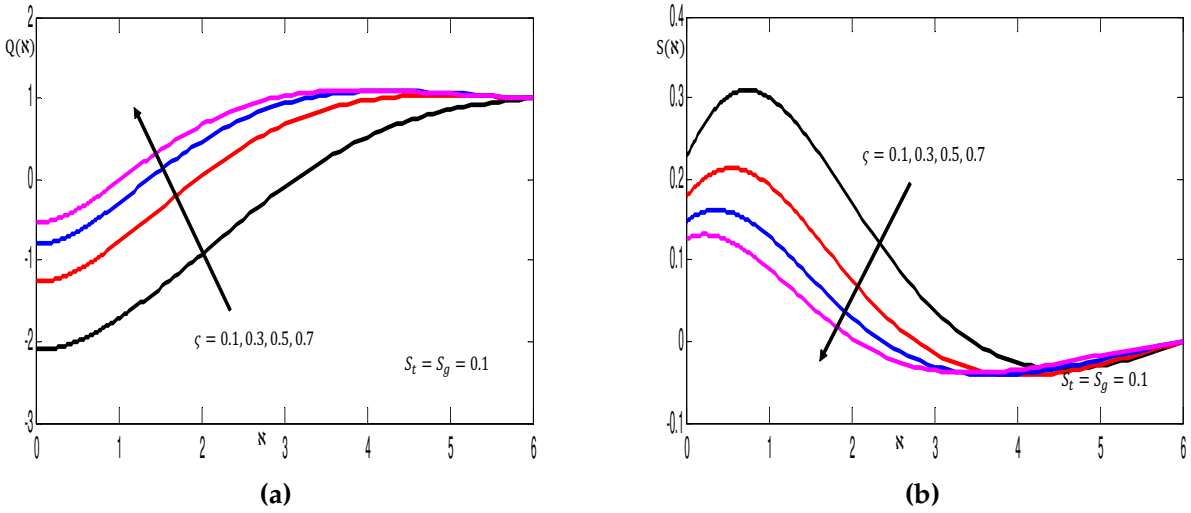

Figure 9. The changes in the **(a)** contribution of ς on concentration distribution of homogeneous bulk fluid and **(b)** contribution of ς on concentration distribution of heterogeneous catalyst at the surface

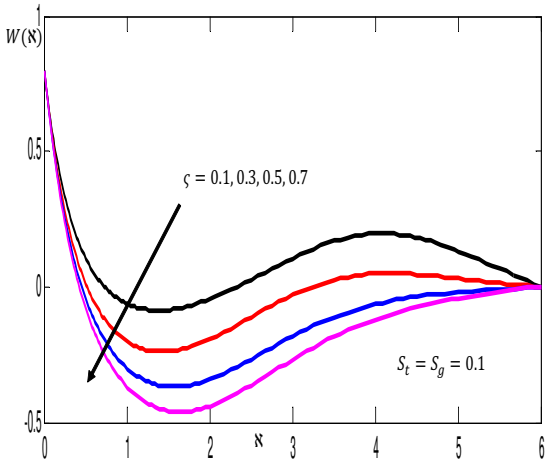

Figure 10. Contribution of ς on bioconvection distribution

The variations in profiles of concentration of reactant A and concentration of reactant B with increasing values of homogeneous reaction material $\mathcal{R}$ are computed in Figs. 11(a) and 11(b) when $S_t = S_g = 0.1$. It is discovered that an increase in the magnitude of $\mathcal{R}$ produces a significant increase in the concentration of reactant A and a slight elevation is deduced in the concentration of reactant B at the hypolimnion stratified layer of the upper horizontal surface of the paraboloid of revolution.

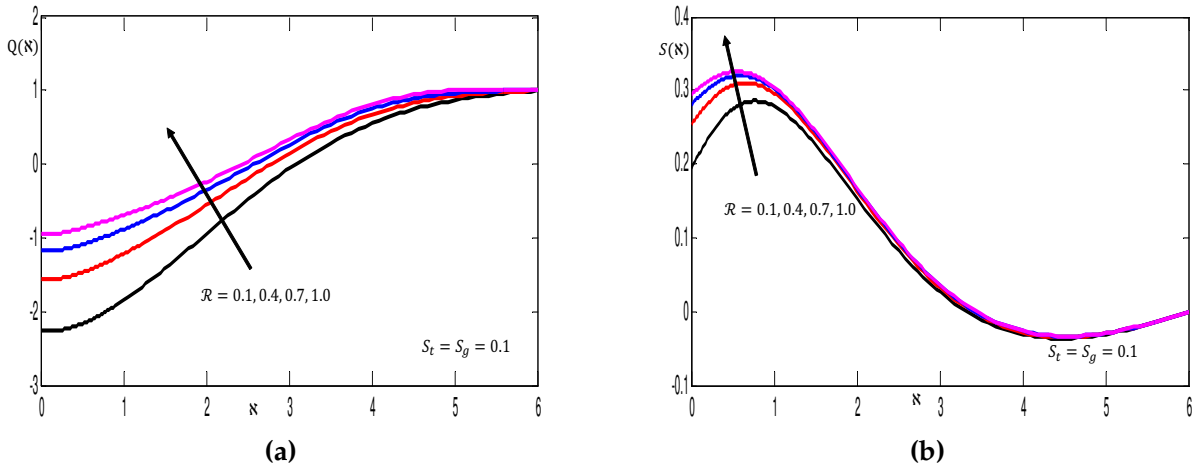

Figure 11. The changes in the **(a)** Contribution of $\mathcal{R}$ on concentration distribution of homogeneous bulk fluid and **(b)** contribution of $\mathcal{R}$ on concentration distribution of heterogeneous catalysts at the surface

Figs. 12(a) and 12(b) delineates impact of heterogeneous reaction parameter $\mathcal{J}$ on profiles of concentration of reactant A and concentration of reactant B when $S_t = S_g = 0.1$ and $\mathcal{R} = 1.0$. It is seen from the Fig. 12(a) that concentration of reactant A is an increasing function of $\mathcal{J}$ while in Fig. 12(b) it is noticed that the concentration of reactant B is a decreasing function of $\mathcal{J}$.

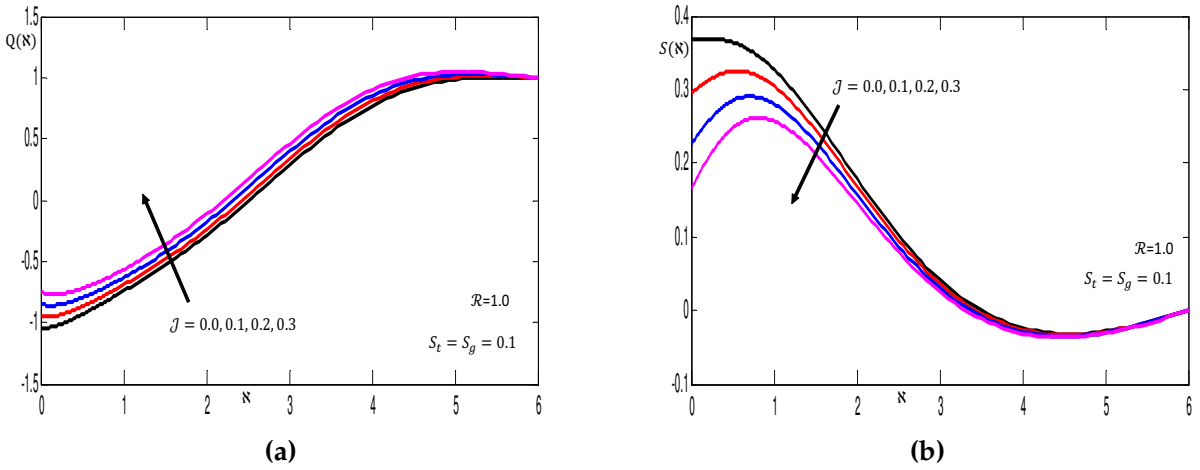

Figure 12. The changes in the **(a)** contribution of $\mathcal{J}$ on concentration distribution of homogeneous bulk fluid and **(b)** contribution of $\mathcal{J}$ on concentration distribution of heterogeneous catalysts at the surface

The impact of the bioconvection Schmidt number S_{cm} is plotted in Fig. 13 when $S_t = S_g = 0.1$ and $\beth = 2.0$. It is seen that the bioconvection distribution exhibits decelerating characteristics within the domain $0 \leq \aleph \leq 2.4$ and further shows a diminution within the domain $2.8 \leq \aleph \leq 6.0$ of the upper horizontal surface of a paraboloid of revolution when S_{cm} is raised. Physically, the observed development is attributable to the fact that the bioconvection Schmidt number S_{cm} corresponds to the ratio of momentum diffusivity to the diffusivity of microorganisms. It is worth noting that, raising S_{cm} correlates to a decrease in microorganisms' diffusion, which reduces both the density and the thickness of the boundary layer for motile microorganisms.

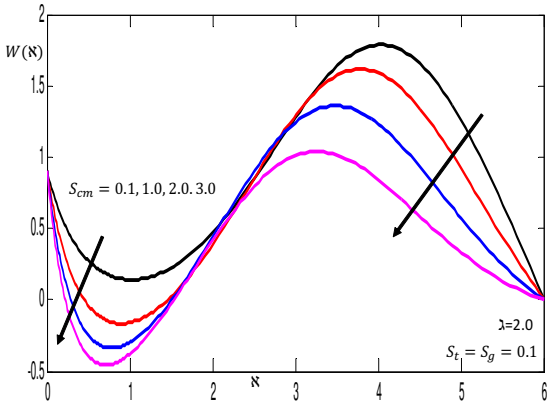

Figure 13. Contribution of S_{cm} on bioconvection distribution

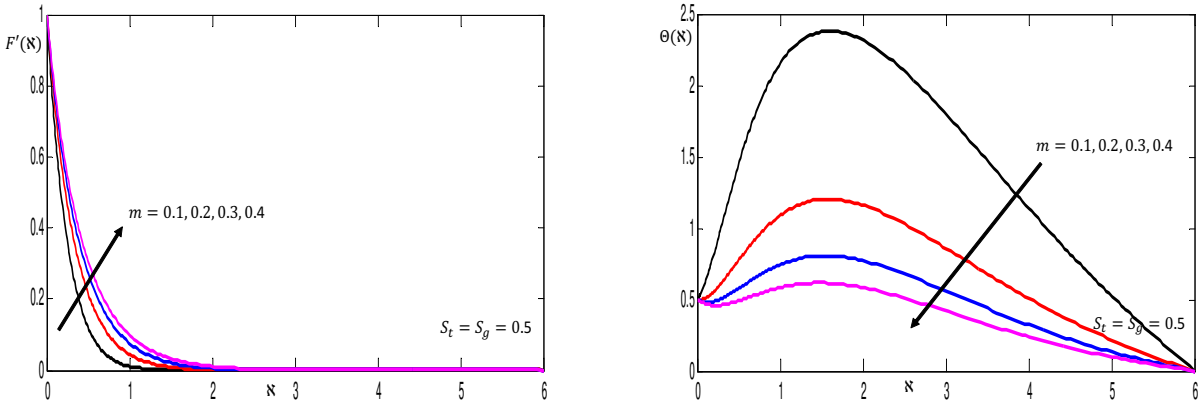

Figure 14. The changes in the **(a)** contribution of m on velocity distribution and **(b)** contribution of m on temperature distribution

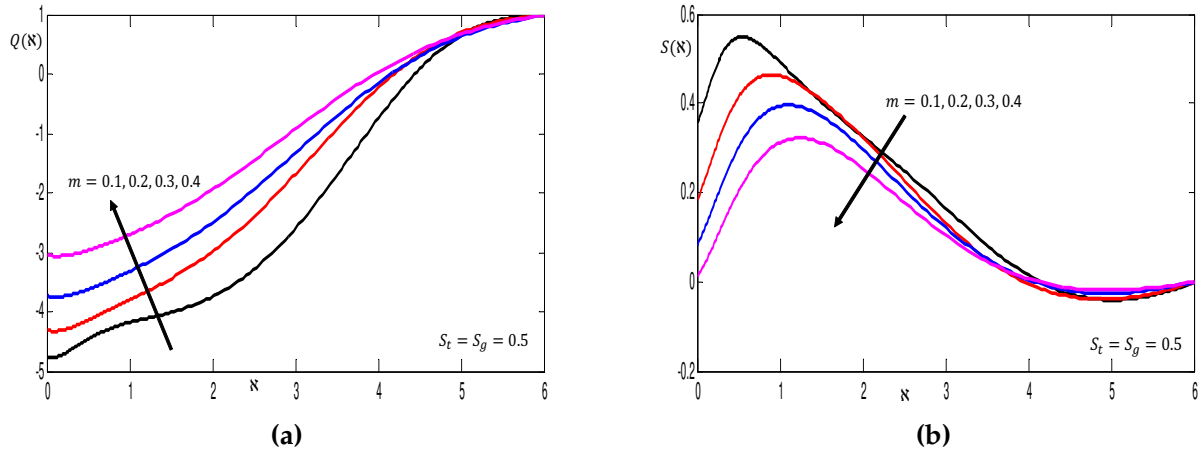

Figure 15. The changes in the **(a)** contribution of m on concentration distribution of homogeneous bulk fluid and **(b)** contribution of m on concentration distribution of heterogeneous catalysts at the surface

The effect of the velocity index parameter m is revealed in Figs. 14-15 when $S_t = S_g = 0.5$. It is noticed in Fig. 14(a) that incremental values of m lead to augmentation of the velocity distribution while a decline in the temperature distribution is noticed in Fig. 14(b). In Fig. 15(a)-15(b) it is obvious that the concentration of homogeneous (bulk fluid) and concentration of heterogeneous (catalyst at the surface) are increasing and decreasing functions of m respectively. Figs. 16(a)-17(a) are plotted to view the variations in the concentration of homogeneous (bulk fluid), concentration of heterogeneous (catalyst at the surface), and bioconvection distribution with rising values of thermophoretic parameter $N_t(N_t = 0.1,\ 0.2,\ 0.3,\ 0.4)$. In Fig. 16(a), it is envisioned that within the domain $0 \leq \aleph \leq 2.7$ a diminution is noticed in the concentration of homogeneous (bulk fluid) for larger values of N_t and thereafter an enhancement is observed for $2.8 \leq \aleph \leq 6.0$. While in Fig. 16(b) a quite different behaviour is envisioned in the aspect of concentration of homogenous catalyst at the surface in the sense that, as N_t is raised, there is a substantial enhancement within the domain $0 \leq \aleph \leq 2.7$ of the concentration of heterogeneous catalyst at the surface and decline is later noticed when $2.8 \leq \aleph \leq 6.0$. Physically, the apparent trend results from the abrupt movement of heated particles from a location of high heat energy to a region of low heat energy in thermophoresis. In reality, thermophoresis may be witnessed in a heated fluorescent bulb, where heated particles tend to move to a location with a lower temperature gradient. In Fig. 17(a) it is observed that incremental values of N_t lead to an enhancement of the bioconvection distribution. Figs. 17(b)-18 present the influence of Brownian motion parameter N_b on the concentration of homogeneous bulk fluid and concentration of heterogeneous catalyst at the surface, respectively. In Fig. 17(b) it is observed that there is an obvious augmentation in the concentration of homogeneous bulk fluid with an increment in $N_b(N_b = 0.1,\ 0.2,\ 0.3,\ 0.4)$. Physically, these characteristics result from the collision of particles caused by the random motion of nanoparticles within the wall of the upper horizontal surface of the paraboloid of rotation. As a result of this development, kinetic energy is converted into thermal energy, resulting in improved behavior of homogenous concentrations (bulk fluid). In Fig. 18, a decline effect is noticed in the concentration of heterogeneous catalyst at the surface when N_b is raised, thereafter within the domain $3.4 \leq \aleph \leq 6.0$ a slight augmentation is noticed towards the freestream.

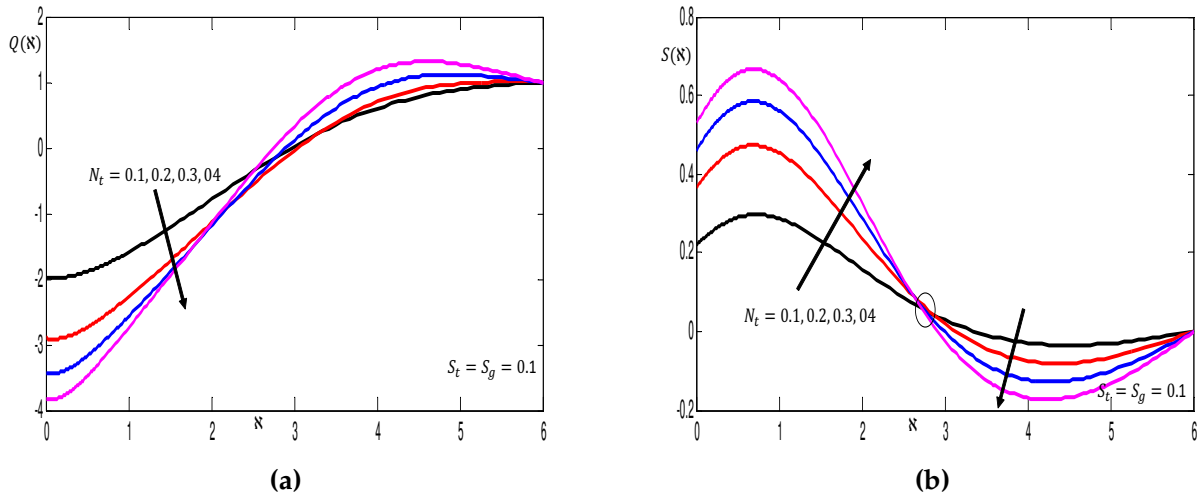

Figure 16. The changes in the **(a)** contribution of N_t on concentration distribution of homogeneous bulk fluid and **(b)** contribution of N_t on concentration distribution of heterogeneous catalysts at the surface

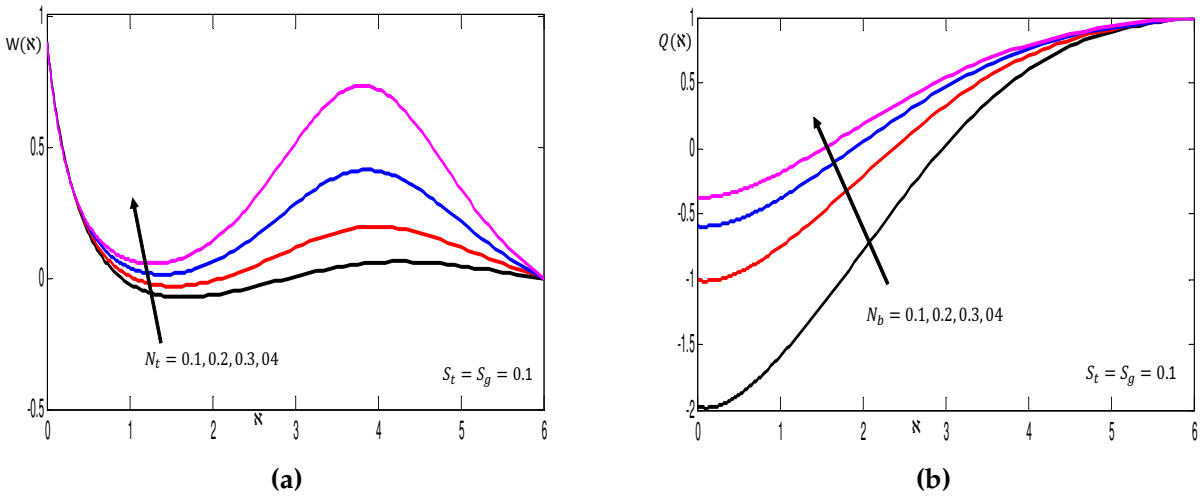

Figure 17. The changes in the **(a)** contribution of N_t on bioconvection distribution and **(b)** contribution of N_b on concentration distribution of homogeneous bulk fluid

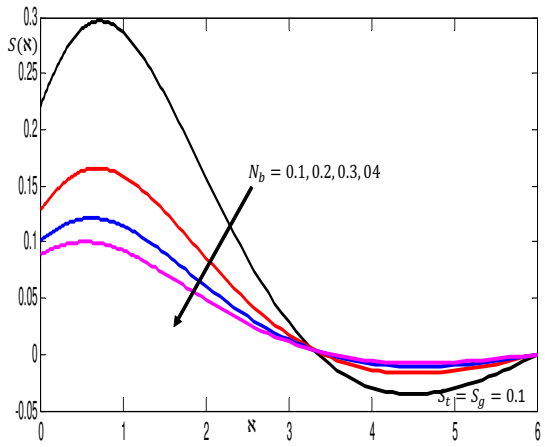

Figure 18. The changes in the contribution of N_b on concentration distribution of heterogeneous catalysts at the surface

Figs. 19-20 are prepared to demonstrate the significance of Prandtl number P_r when $S_t = S_g = 0.1$. In Fig. 19(a), increasing values of $P_r (P_r = 0.1,\ 0.7,\ 1.5,\ 2.0)$ cause the diminution of temperature distribution. It is physically justifiable since the Prandtl number represents the connection between a fluid's momentum transfer and thermal transport capacity.
In other words, Prandtl number $P_r = \frac{\vartheta}{\alpha} = \frac{\frac{\mu}{\rho}}{\frac{k}{\rho C_p}}$ reveals the relationship between kinematic viscosity and thermal diffusivity of the fluid. Therefore as P_r increases the viscosity of the Erying-Powel fluid magnifies leading to declining in the temperature of the fluid as it flows along the upper horizontal surface of a paraboloid of revolution. The impact of P_r on $Q(ℵ)$ is manifested in Fig. 19(b). It is observed that an increment in P_r corresponds to the decline in the concentration of homogeneous bulk fluid. In Fig. 20(a), an increase in P_r leads to the enhancement of the concentration of heterogeneous catalyst at the surface. Likewise, from Fig. 20(b) it is observed that the concentration of bioconvection lifts up as P_r is raised.

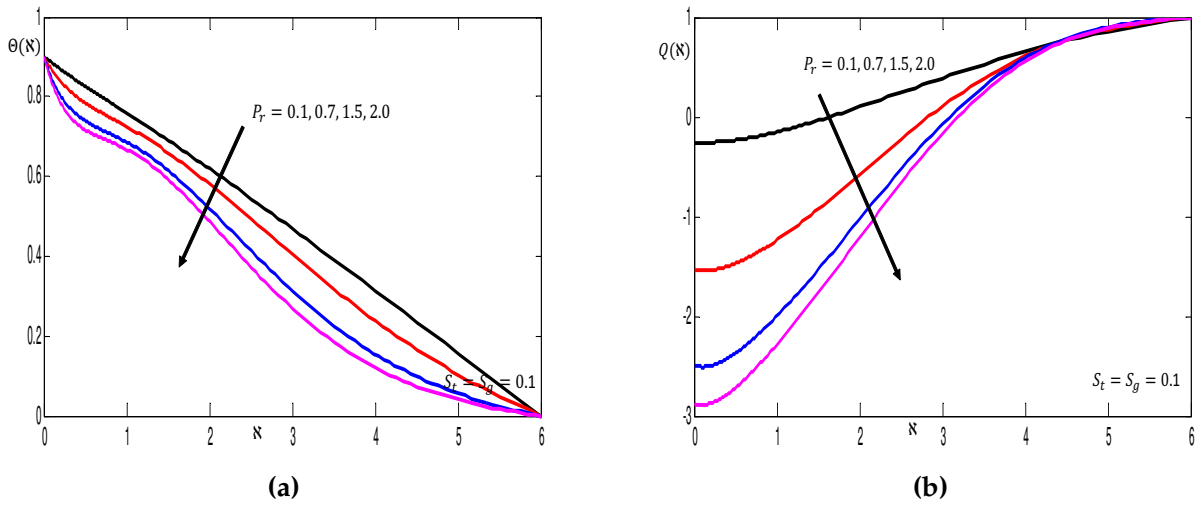

Figure 19. The changes in the **(a)** contribution of P_r on temperature distribution and **(b)** contribution of P_r on concentration distribution of homogeneous bulk fluid

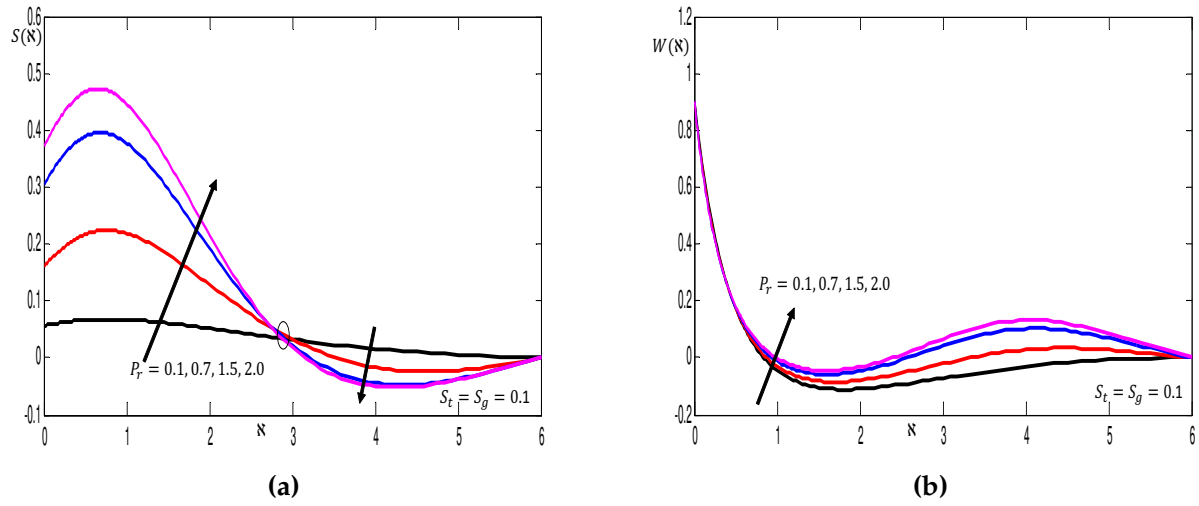

Figure 20. The changes in the **(a)** contribution of P_r on concentration distribution of heterogeneous catalysts at the surface and **(b)** contribution of P_r on bioconvection distribution

Figs. 21(a)-21(b) demonstrate the behavior of temperature-dependent viscous parameter ξ and temperature-dependent thermal conductivity parameter on velocity and temperature distributions, respectively. In Fig. 21(a), it revealed that the velocity distribution is enhanced with higher ξ, likewise with elevation in ε as seen in Fig. 21(b), there is a well-pronounced augmentation in the temperature distribution. Physically, this observation is a result of the fact that increasing thermal conductivity causes the kinetic energy of the fluid particles to increase, thus enhancing the temperature of the fluid. Figs. 22(a) and 22(b) present the effect of Prandtl number P_r on skin friction coefficient $Cf_x(Re_x)^{\frac{1}{2}}$ and Nusselt number $Nu_x(Re_x)^{-\frac{1}{2}}$, respectively. It is envisioned that both $Cf_x(Re_x)^{\frac{1}{2}}$ and $Nu_x(Re_x)^{-\frac{1}{2}}$ encumber with increasing P_r.

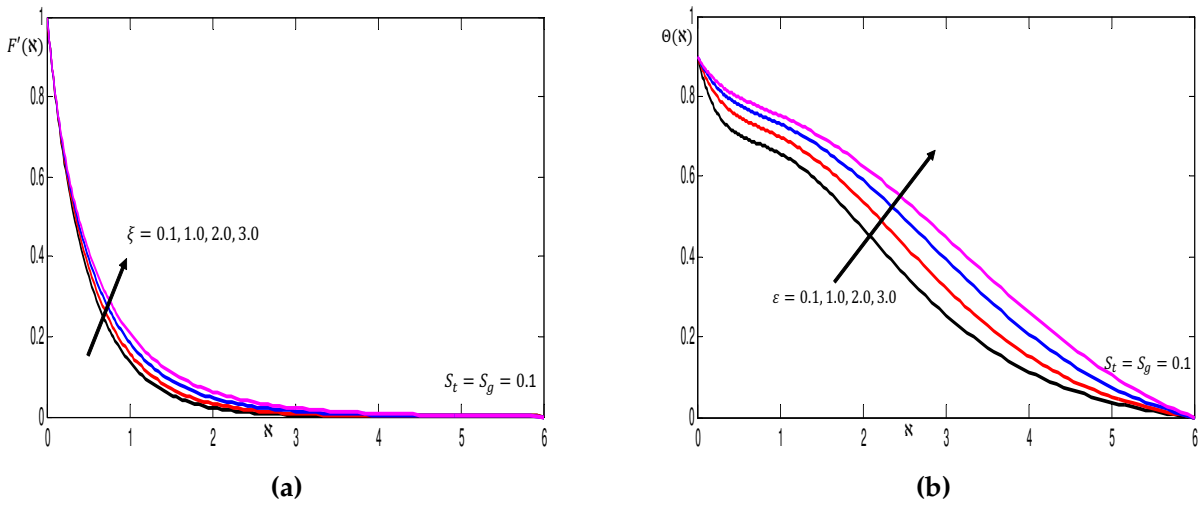

Figure 21. **(a)** Contribution of ξ on velocity distribution and **(b)** contribution of ε on temperature distribution

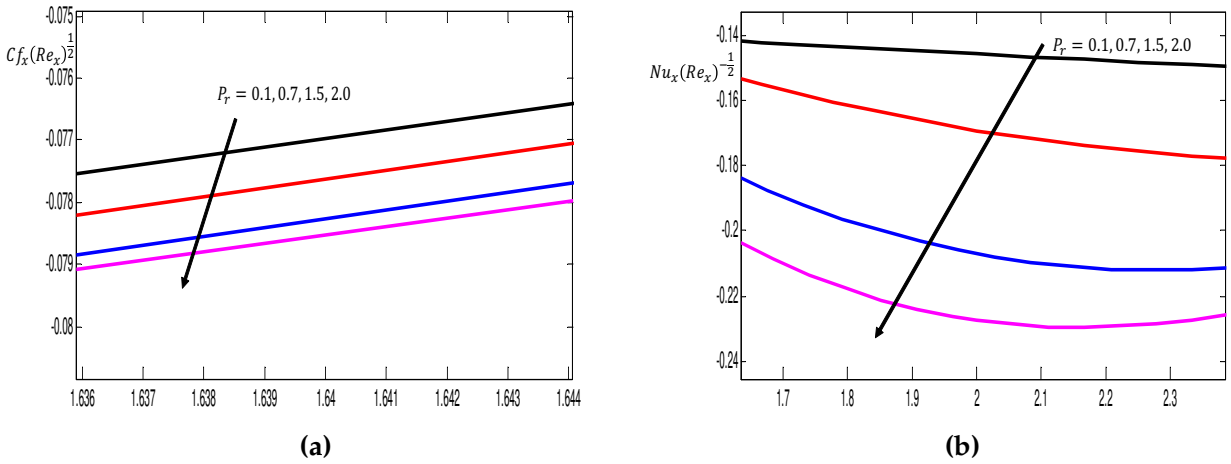

Figure 22. The changes in the **(a)** contribution of P_r on on coefficient of skin friction and **(b)** contribution of P_r on Nusselt number

5 Conclusions

The use of catalytic reactions in industry and real-life applications offers numerous economic advantages which include improved process efficiency, reduced energy consumption, and reduced waste production making it a critical tool for achieving sustainable and cost-effective chemical production. The motion of air across the pointed surface of an aircraft or over the bonnet of a car is highly important to scientists. Geometrically, the motion of fluid over this particular domain is termed the upper horizontal surface of a paraboloid of revolution. Simulation has been carried out for the boundary layer flow of Erying-Powell fluid transporting nanoparticles in the presence of stratifications and varying fluid characteristics across a surface with variable thickness. Thermal stratification, microorganisms stratification, and variable fluid properties have been appropriately modeled. When material parameters are increased, it is concluded that the viscosity of fluid subsides at the lowest layer of stratification, and the motion of Erying-

Powel increases across the upper horizontal surface of the paraboloid of revolution. Increasing the magnitude of Darcy-Forchheimer parameters corresponds to the diminution of velocity distribution and augmentation of temperature distribution. An improvement in bioconvection distribution is shown as the thermophoretic parameter is elevated. With increasing Brownian motion parameters, the homogeneous bulk fluid displays substantial augmentation. When the temperature-dependent viscosity parameter and temperature-dependent thermal conductivity parameter are raised, the fluid's velocity and temperature are increased. Significant enhancement is noticed in both temperature distribution and concentration distribution of heterogeneous catalysts at the surface when heat generation is increased. It is therefore significant to state that the major influence of these germane parameters would go a long way towards assisting scientists in reaching efficiency in the course of production in industries.

The present work can be extended to hybrid nanofluids. The combined effect of nonlinear thermal radiation and stratification can be properly incorporated which has many applications in the industry.

Declarations

Ethical approval

Not applicable.

Consent for publication

Not applicable.

Conflicts of interest

The authors declare that they have no conflict of interest.

Author's contributions

A.O.P.: Conceptualization, Supervision, Project Administration. T.O.: Formal Analysis, Investigation, Data Curation, Writing-Original Draft, Writing-Review & Editing. N.A.S.: Conceptualization, Formal Analysis, Resources, Visualization, Acquisition. E.O.: Methodology, Writing-Original Draft, Validation Project Administration, M.M.A.: Software, Validation, Data Curation, Writing-Review & Editing. All authors discussed the results and contributed to the final manuscript.

Acknowledgements

Not applicable.

References

[1] Shamshuddin, M.D., Shahzad, F., Jamshed, W., Bég, O.A., Eid, M.R. and Bég, T.A. Thermo-solutal stratification and chemical reaction effects on radiative magnetized nanofluid flow along an exponentially stretching sensor plate: Computational analysis. *Journal of Magnetism and Magnetic Materials*, 565, 170286, (2023). [CrossRef]

[2] Tamilzharasan, B.M., Karthikeyan, S., Kaabar, M.K., Yavuz, M. and Özköse, F. Magneto mixed convection of Williamson nanofluid flow through a double stratified porous medium in attendance of activation energy. *Mathematical and Computational Applications*, 27(3), 46, (2022). [CrossRef]

[3] Jagan, K. and Sivasankaran, S. Soret & Dufour and Triple stratification effect on MHD flow

with velocity slip towards a stretching cylinder. *Mathematical and Computational Applications*, 27(2), 25, (2022). [CrossRef]

[4] Rehman, S., Anjum, A., Farooq, M., Hashim and Malik, M.Y. Melting heat phenomenon in thermally stratified fluid reservoirs (Powell-Eyring fluid) with joule heating. *International Communications in Heat and Mass Transfer,* 137, 106196, (2022). [CrossRef]

[5] Oreyeni, T., Ramesh, K., Nayak, M.K. and Oladele, P.A. Triple stratification impacts on an inclined hydromagnetic bioconvective flow of micropolar nanofluid with exponential space-based heat generation. *Waves in Random and Complex Media*. [CrossRef]

[6] Fayz-Al-Asad, M., Oreyeni, T., Yavuz, M. and Olanrewaju, P.O. Analytic simulation of MHD boundary layer flow of a chemically reacting upper-convected Maxwell fluid past a vertical surface subjected to double stratifications with variable properties. *The European Physical Journal Plus,* 137, 813, (2022). [CrossRef]

[7] Khan, W.A., Anjum, N., Waqas, M., Abbas, S.Z., Irfan, M. and Muhammad, T. Impact of stratification phenomena on a nonlinear radiative flow of sutterby nanofluid. *Journal of Materials Research and Technology,* 15, 306-314, (2021). [CrossRef]

[8] Chen, S.B., Shahmir, N., Ramzan, M., Sun, Y.L., Aly, A.A. and Malik, M.Y. Thermophoretic particle deposition in the flow of dual stratified Casson fluid with magnetic dipole and generalized Fourier's and Fick's laws. *Case Studies in Thermal Engineering*, 26, 101186, (2021). [CrossRef]

[9] Dawar, A., Shah, Z., Alshehri, H. M., Islam, S. and Kumam, P. Magnetized and non-magnetized Casson fluid flow with gyrotactic microorganisms over a stratified stretching cylinder. *Scientific Reports*, 11, 16376, (2021). [CrossRef]

[10] Verma, A.K., Bhattacharyya, K., Rajput, S., Mandal, M.S., Chamkha, A.J. and Yadav, D. Buoyancy driven non-Newtonian Prandtl-Eyring nanofluid flow in Darcy-Forchheimer porous medium over inclined non-linear expanding sheet with double stratification. *Waves in Random and Complex Media*, (2022). [CrossRef]

[11] Mahmood, Z., Alhazmi, S.E., Alhowaity, A., Marzouki, R., Al-Ansari, N. and Khan, U. MHD mixed convective stagnation point flow of nanofluid past a permeable stretching sheet with nanoparticles aggregation and thermal stratification. *Scientific Reports,* 12, 16020, (2022). [CrossRef]

[12] Koriko, O.K., Shah, N.A., Saleem, S., Chung, J.D., Omowaye, A.J. and Oreyeni, T. Exploration of bioconvection flow of MHD thixotropic nanofluid past a vertical surface coexisting with both nanoparticles and gyrotactic microorganisms. *Scientific Reports,* 11, 16627, (2021). [CrossRef]

[13] Shah, N.A., Tosin, O., Shah, R., Salah, B. and Chung, J.D. Brownian motion and thermophoretic diffusion effects on the dynamics of MHD upper convected Maxwell nanofluid flow past a vertical surface. *Physica Scripta,* 96(12), 125722, (2021). [CrossRef]

[14] Nadeem, S., Fuzhang, W., Alharbi, F.M., Sajid, F., Abbas, N., El-Shafay, A.S. and Al-Mubaddel, F.S. Numerical computations for Buongiorno nano fluid model on the boundary layer flow of viscoelastic fluid towards a nonlinear stretching sheet. *Alexandria Engineering Journal,* 61(2), 1769-1778, (2022). [CrossRef]

[15] Rao, A.S., Ramaiah, K.D., Kotha, G., Rao, M.V.S. and Chamkha, A.J. A Spectral Relaxation approach for boundary layer flow of nanofluid past an exponentially stretching surface with variable suction in the presence of heat source/sink with viscous dissipation. *Arabian Journal*

for Science and Engineering, 46, 7509-7520, (2021). [CrossRef]

[16] Ur Rasheed, H., AL-Zubaidi, A., Islam, S., Saleem, S., Khan, Z. and Khan, W. Effects of Joule heating and viscous dissipation on magnetohydrodynamic boundary layer flow of Jeffrey nanofluid over a vertically stretching cylinder. *Coatings*, 11(3), 353, (2021). [CrossRef]

[17] Abbas, Z., Abdal, S., Hussain, N., Hussain, F., Adnan, M., Ali, B., ... & Younas, S. (2019). Mhd boundary layer flow and heat transfer of nanofluid over a vertical stretching sheet in the presence of a heat source. *Scientific Inquiry and Review*, 3(4), 60-73, (2019). [CrossRef]

[18] Rasool, G., Shafiq, A. and Durur, H. Darcy-Forchheimer relation in magnetohydrodynamic Jeffrey nanofluid flow over stretching surface. *Discrete & Continuous Dynamical Systems Series S*, 14(7), 2497-2515, (2021). [CrossRef]

[19] Kebede, T., Haile, E., Awgichew, G. and Walelign, T. Heat and mass transfer in unsteady boundary layer flow of Williamson nanofluids. *Journal of Applied Mathematics*, 1890972, (2020). [CrossRef]

[20] Swain, K., Mahanthesh, B. and Mebarek-Oudina, F. Heat transport and stagnation-point flow of magnetized nanoliquid with variable thermal conductivity, Brownian moment, and thermophoresis aspects. *Heat Transfer*, 50(1), 754-767, (2021). [CrossRef]

[21] Qureshi, M.A. Numerical simulation of heat transfer flow subject to MHD of Williamson nanofluid with thermal radiation. *Symmetry*, 13(1), 10, (2021). [CrossRef]

[22] Sravanthi, C.S., Mabood, F., Nabi, S. G. and Shehzad, S.A. Heterogeneous and homogeneous reactive flow of magnetite-water nanofluid over a magnetized moving plate. *Propulsion and Power Research*, 11(2), 265-275, (2022). [CrossRef]

[23] Alzahrani, F., Growda, R.J.P., Kumar, R.N. and Khan, M.I. Dynamics of thermosolutal Marangoni convection and nanoparticle aggregation effects on Oldroyd-B nanofluid past a porous boundary with homogeneous-heterogeneous catalytic reactions. *Journal of the Indian Chemical Society*, 99(6), 100458, (2022). [CrossRef]

[24] Sarojamma, G., Lakshmi, R.V., Narayana, P.V.S. and Animasaun, I.L. Exploration of the significance of autocatalytic chemical reaction and Cattaneo-Christov heat flux on the dynamics of a micropolar fluid. *Journal of Applied and Computational Mechanics*, 6(1), 77-89, (2020). [CrossRef]

[25] Animasaun, I.L., Mahanthesh, B., Sarojamma, G. and Damisa, J.S. Significance of thickness of paraboloid of revolution and buoyancy forces on the dynamics of Erying-Powel fluid subject to equal diffusivity kind of quartic autocatalysis. *Physica A: Statistical Mechanics and its Applications*, 549, 124047, (2020). [CrossRef]

[26] Hayat, T., Hussain, Z., Muhammad, T. and Alsaedi, A. Effects of homogeneous and heterogeneous reactions in flow of nanofluids over a nonlinear stretching surface with variable surface thickness. *Journal of Molecular Liquids*, 221, 1121-1127, (2016). [CrossRef]

[27] Zhao, Q., Xu, H. and Tao, L. Homogeneous-heterogeneous reactions in boundary-layer flow of a nanofluid near the forward stagnation point of a cylinder. *Journal of Heat Transfer*, 139(3), 034502, (2016). [CrossRef]

[28] Platt, J.R. Bioconvection patterns in cultures of free-swimming organisms. *Science*, 133(3466), 1766-1767, (1961). [CrossRef]

[29] Ramzan, M., Shamshad, U., Rehman, S., Saeed, A., Kumam, P. and Watthayu, W. Compuation of MHD flow of three-dimensional mixed convection non-Newtonian viscoelastic fluid with the physical aspect of gyrotactic microorganism. *Waves in Random and Complex Media*, 1-23, (2022). [CrossRef]

[30] Zhang, L., Puneeth, V., Ijaz Khan, M., El-Zahar, E.R., Manjunath, N., Shah, N.A., Chung, J.D., Khan, S.U. and Khan, M.I. Applications of bioconvection for tiny particles due to two concentric cylinders when role of Lorentz force is significant. *Plos One,* 17(5), e0265026, (2022). [CrossRef]

[31] Rao, M.V.S., Gangadhar, K., Chamkha, A.J. and Surekha, P. Bioconvection in a convectional nanofluid flow containing gyrotactic microorganisms over an isothermal vertical cone embedded in a porous surface with chemical reactive species. *Arabian Journal for Science and Engineering,* 46, 2493-2503, (2021). [CrossRef]

[32] Sankad, G., Ishwar, M. and Dhange, M. Varying wall temperature and thermal radiation effects on MHD boundary layer liquid flow containing gyrotactic microorganisms. *Partial Differential Equations in Applied Mathematics,* 4, 100092, (2021). [CrossRef]

[33] Parveen, N., Awais, M., Awan, S.E., Shah, S.A., Yuan, A., Nawaz, M., Akhtar, R. and Malik, M.Y. Thermophysical properties of chemotactic microorganisms in bio-convective peristaltic rheology of nano-liquid with slippage, Joule heating and viscous dissipation. *Cases in Thermal Engineering,* 27, 101285, (2021). [CrossRef]

[34] Naganthran, K., Md Basir, M.F., Thumma, T., Ige, E.O., Nazar, R. and Tlili, I. Scaling group analysis of bioconvective micropolar fluid flow and heat transfer in a porous medium. *Journal of Thermal Analysis and Calorimetry,* 143, 1943-1955, (2021). [CrossRef]

[35] Ramzan, M., Bilal, M., Kanwal, S. and Chung, J.D. Effects of variable thermal conductivity and non-linear thermal radiation past an Eyring Powell nanofluid with chemical reaction. *Communications in Theoretical Physics,* 67(6), 723-731, (2017). [CrossRef]

[36] Hayat, T., Iqbal, Z., Qasim, M. and Alsaedi, A. Flow of an Eyring-Powell fluid with convective boundary conditions. *Journal of Mechanics,* 29(2), 217-224, (2013). [CrossRef]

[37] Animasaun, L. and Koriko, O.K. New similarity solution of micropolar fluid flow problem over an UHSPR in the presence of quartic kind of autocatalytic chemical reaction. *Frontiers in Heat and Mass Transfer,* 8(26), (2017). [CrossRef]

[38] Kuznetsov, A.V. and Nield, D.A. Double-diffusive natural convective boundary layer flow of a nanofluid past a vertical plate. *International Journal of Thermal Sciences,* 50(5), 712-717, (2011). [CrossRef]

[39] Raees, A., Xu, H., Sun, Q. and Pop, I. Mixed convection in gravity-driven nanoliquid film containing both nanoparticles and gyrotactic microorganisms. *Applied Mathematics and Mechanics,* 36(2), 163-178, (2015). [CrossRef]

[40] Chaudhary, M.A. and Merkin, J.H. A simple isothermal model for homogeneous-heterogeneous reaction in boundary-layer flow. I Equal diffusivities. *Fluid Dynamics Research,* 16(6), 311-333, (1995). [CrossRef]

[41] Koriko, O.K., Omowaye, A.J., Sandeep, N. and Animasaun, I.L. Analysis of boundary layer formed on an upper horizontal surface of a paraboloid of revolution within nanofluid flow in the presence of thermophoresis and Brownian motion of 29 nm CuO. *International Journal of Mechanical Sciences,* 124-125, 22-36, (2017). [CrossRef]

[42] Kuznetsov, A.V. The onset of nanofluid bioconvection in a suspension containing both nanoparticles and gyrotactic microorganisms. *International Communications in Heat and Mass Transfer,* 37(10), 1421-1425, (2010).[CrossRef]

[43] Batchelor, G.K. *An Introduction to Fluid Dynamics*. Cambridge University Press: London, (1987).

[44] Charraudeau, J. Influence de gradients de proprietes physiques en convection forcee-application au cas du tube. *International Journal of Heat and Mass Transfer,* 18(1), 87-95, (1975). [CrossRef]

[45] Oreyeni, T., Shah, N.A., Popoola, A.O., Elzahar, E.R. and Yook, S.J. The significance of exponential space-based heat generation and variable thermophysical properties on the dynamics of Casson fluid over a stratified surface with non-uniform thickness. *Waves in Random and Complex Media*, (2022). [CrossRef]

[46] Oreyeni, T. and Omokhuale, E. Optimal homotopy analysis of MHD natural convection flow of thixotropic fluid under subjection of thermal stratification: Boundary layer analysis. *American Journal of Computational Mathematics,* 9(02), 116-131, (2019). [CrossRef]

[47] Koriko, O.K., Animasaun, I.L., Omowaye, A.J. and Oreyeni, T. The combined influence of nonlinear thermal radiation and thermal stratification on the dynamics of micropolar fluid along a vertical surface. *Multidiscipline Modeling in Materials and Structures,* 15(1), 133-155, (2019). [CrossRef]

[48] Koriko, O.K., Oreyeni, T., Omowaye, A.J. and Animasaun, I.L. Homotopy analysis of MHD free convective micropolar fluid flow along a vertical surface embedded in non-darcian thermally-stratified medium. *Open Journal of Fluid Dynamics,* 6(3), 198-221, (2016). [CrossRef]

Mathematical Modelling and Numerical Simulation with Applications (MMNSA)
(https://dergipark.org.tr/en/pub/mmnsa)

How to cite this article: Shah, N.A., Popoola, A.O., Oreyeni, O., Omokhuale, E., & Altine, M.M. (2023). A modelling of bioconvective flow existing with tiny particles and quartic autocatalysis reaction across stratified upper horizontal surface of a paraboloid of revolution. *Mathematical Modelling and Numerical Simulation with Applications,* 3(1), 74-100. https://doi.org/10.53391/mmnsa.1280184